CPIA PUBLICATION 502
DECEMBER 1988

HIGH-STRAIN RATE TESTING OF GUN PROPELLANTS

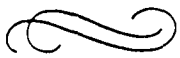

Harry J. Hoffman

CHEMICAL PROPULSION INFORMATION AGENCY
Operating under contract N00039-87-C-5301
THE JOHNS HOPKINS UNIVERSITY · APPLIED PHYSICS LABORATORY · LAUREL, MD.

UNCLASSIFIED

SECURITY CLASSIFICATION OF THIS PAGE

REPORT DOCUMENTATION PAGE

1a REPORT SECURITY CLASSIFICATION UNCLASSIFIED	1b RESTRICTIVE MARKINGS
2a SECURITY CLASSIFICATION AUTHORITY	3 DISTRIBUTION / AVAILABILITY OF REPORT Approved for public release; distribution is unlimited.
2b DECLASSIFICATION / DOWNGRADING SCHEDULE	
4 PERFORMING ORGANIZATION REPORT NUMBER(S) CPIA Publication 502	5 MONITORING ORGANIZATION REPORT NUMBER(S)
6a NAME OF PERFORMING ORGANIZATION Johns Hopkins University Applied Phys Lab Chem Prop Inf Agy 6b OFFICE SYMBOL (If applicable) CPIA	7a NAME OF MONITORING ORGANIZATION Space and Naval Warfare Systems Command
6c ADDRESS (City, State, and ZIP Code) Laurel, MD 20707	7b ADDRESS (City, State, and ZIP Code) Washington, DC 20363
8a NAME OF FUNDING / SPONSORING ORGANIZATION DLA/DTIC 8b OFFICE SYMBOL (If applicable) DTIC-DF	9 PROCUREMENT INSTRUMENT IDENTIFICATION NUMBER N00039-87-C-5301
8c ADDRESS (City, State, and ZIP Code) Cameron Station Alexandria, VA 22314	10 SOURCE OF FUNDING NUMBERS (For Basic Mission) PROGRAM ELEMENT NO: 65802 S; PROJECT NO: 1.0; TASK NO:; WORK UNIT ACCESSION NO:

11 TITLE (Include Security Classification)
High-Strain Rate Testing of Gun Propellants

12 PERSONAL AUTHOR(S)
Hoffman, Harry J.

13a TYPE OF REPORT	13b TIME COVERED	14 DATE OF REPORT (Year, Month, Day)	15 PAGE COUNT
Final	FROM 010188 TO 103188	1988 December	72

16 SUPPLEMENTARY NOTATION
CPIA's DTIC-assigned source code is 081100.

Reproduction not authorized except by specific permission from CPIA.

17 COSATI CODES			18 SUBJECT TERMS (Continue on reverse if necessary and identify by block number)
FIELD	GROUP	SUB-GROUP	
19	01		Brittleness, Dynamic response,
14	02		Compressive properties, Fracture (mechanics). (JES)
			Double base gun propellants, (Continued on reverse)

19 ABSTRACT (Continue on reverse if necessary and identify by block number)

A Hopkinson split-pressure bar apparatus was used to test JA-2, M30 and HELOVA gun propellants at strain rates of 600-2,000/s. The split-bar apparatus, a device widely used to measure the dynamic mechanical properties of materials, consists of two elastic bars with a specimen sandwiched between them and a means of generating an elastic stress pulse in the bars. The specimen is loaded beyond the elastic range. Instrumentation of the bars allows recording of the strain history in the bars during the test event. The strain history on the input bar gives a record of the strain rate history in the sample. The output bar strain history is proportional to the stress history in the sample.

The data were compared to the results reported in the literature of earlier high strain rate tests on the same propellants. The data were collected to provide an ambient pressure baseline characterization of the propellant formulations.
(Continued on reverse)

20 DISTRIBUTION / AVAILABILITY OF ABSTRACT	21 ABSTRACT SECURITY CLASSIFICATION
☒ UNCLASSIFIED/UNLIMITED ☐ SAME AS RPT ☐ DTIC USERS	UNCLASSIFIED
22a NAME OF RESPONSIBLE INDIVIDUAL Robert F. Cassel	22b TELEPHONE (Include Area Code) (202) 692-0514
	22c OFFICE SYMBOL NAVSEA-06APR

DD FORM 1473, 84 MAR 83 APR edition may be used until exhausted
All other editions are obsolete

SECURITY CLASSIFICATION OF THIS PAGE
UNCLASSIFIED

18. SUBJECT TERMS (Continued)

Gun propellants	Impulse loading
High pressure	Mechanical properties
Impact tests	Test equipment

19. ABSTRACT (Continued)

A high pressure test facility was designed to expand the test environment for gun propellants to an environment more like that extant during a gun firing. The apparatus is a modification of the common Kolsky version of the Hopkinson split bar that allows pressurization to as much as 200 MPa (30,000 psi). A gas pressurization system was selected to minimize the time required to prepare for an individual test.

CPIA PUBLICATION 502
DECEMBER 1988

HIGH-STRAIN RATE TESTING OF GUN PROPELLANTS

Harry J. Hoffman

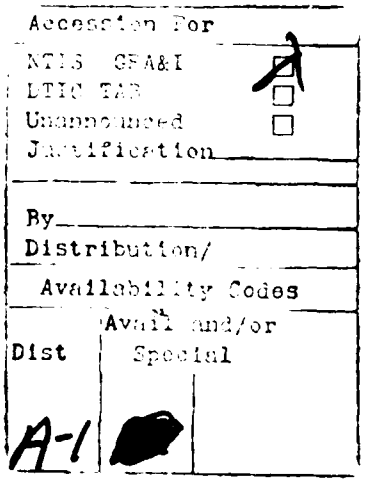

CHEMICAL PROPULSION INFORMATION AGENCY
Operating under contract N00039 87-C 5301
THE JOHNS HOPKINS UNIVERSITY · APPLIED PHYSICS LABORATORY · LAUREL, MD.

The Chemical Propulsion Information Agency (CPIA) is a DoD Information Analysis Center operated by The Johns Hopkins University Applied Physics Laboratory, Johns Hopkins Road, Laurel, Maryland 20707-6099, under Space and Naval Warfare Systems Command Contract N00039-87-C-5301. The applicable DoD Instruction is 3200.12-R-2, "Centers for Analysis of Scientific and Technical Information."

The CPIA also provides technical and administrative support to the Joint Army-Navy-NASA-Air Force (JANNAF) Interagency Propulsion Committee in accordance with DoD Instruction 5030.24, "Interagency Propulsion Committee (Army, Navy, National Aeronautics and Space Administration, Air Force (JANNAF))."

The Government Administrative Manager for CPIA is Mr. Paul Klinefelter, Program Manager for Information Analysis Centers, Defense Technical Information Center, Code DTIC-DF, Cameron Station, Alexandria, Virginia 22304-6145. The Government Technical Manager (Contracting Officer's Technical Representative) is Mr. Robert F. Cassel, Naval Sea Systems Command, NAVSEA-06APR, Washington, DC 20362-5101.

Acknowledgement

The support of Prof. Donald B. Barker, of the Department of Mechanical Engineering, University of Maryland, College Park, and Dr. Robert J. Lieb, of the U.S. Army Ballistics Research Laboratory, Aberdeen Proving Ground, Maryland, is gratefully acknowledged. The research which is the subject of this thesis could not have been completed without their invaluable assistance and encouragement.

Table of Contents

Introduction

The mechanical properties of gun propellants at high rates of strain are of interest to interior ballisticians, in particular, because of their importance in the control of surface area generation during the ballistic cycle. Gun propellant grains are subjected to impacts in the propellant bed during the ignition phase of a firing. High-strain rates are also imposed by the propagation of a shock wave. The result of such impacts and the response of gun propellant grains to shock waves may result in grain fracture and increases in surface area available for combustion. The importance of gun propellant mechanical properties in propelling charge phenomenology was described by Horst (1981).

This report reviews the literature of high-strain rate testing, presents the theory applicable to the Hopkinson split-bar, high-strain rate test device, presents designs for the ambient pressure and high pressure split-bar devices, and gives test results for several gun propellants.

Chapter 1

High-Strain Rate Tests on Gun Propellants

The properties of some gun propellant formulations under high loading rates have been studied previously (see Fong (1985); et al. (1981); Schubert and Schmitt (1973); Greidanus (1976); Benhaim et al. (1978); Wires et al. (1979); and Pinto et al. (1983)). Most of these studies have been carried out at strain rates of 400/s or less and at ambient pressures. The rates of strain to which the propellant grains will be exposed during an actual ignition may be higher due to the intense impacts resulting from passage of the ignition wave. In addition, the pressure in the gun chamber during the event will be much higher than ambient (to approximately 140 to 700 MPa (20,000-100,000 psi)). In order to simulate the high-strain rate environment in the gun chamber, testing using a Hopkinson split-bar device was conducted with inert propellant simulants and live gun propellant formulations. In addition, a device was designed to allow further testing using a Hopkinson split-bar device under pressures up to 200 MPa (30,000 psi).

In the present paper, an application of the Hopkinson split-pressure bar technique to gun propellant testing is presented. The objectives of the current study are 1) to establish a baseline of high-strain rate properties for three different propellant formulations at ambient pressure; and 2) to develop a high-pressure Hopkinson Split Bar test facility. The high-pressure apparatus is being fabricated at the U.S. Army Ballistic Research Laboratory (BRL) Interior Ballistics Division (IBD) at Aberdeen Proving Ground, Maryland.

Background

The general technique of using a cylindrical bar to transmit a stress pulse to a specimen in order to investigate the properties of the specimen was developed by Hopkinson (1914). Various modifications of the technique have been developed to study the compressive, tensile, and torsional properties of many different types of materials. Common to all these approaches is the transmission of a pulse through elastic media to generate stresses outside the elastic range in the test specimen. Devices have been developed to examine both uniaxial and biaxial properties.

Many modern applications of the technique have been based on the apparatus developed by Kolsky (1949). In his approach, very thin specimens were used to maximize longitudinal propagation of the stress wave, thereby reducing the effort required for data reduction. The thinness of the wafers also maximized strain rate in the specimen, by reflection of stress pulses on the ends of the bars. However the effects of friction at the interface of the specimen and the end of the bar were found to be significant, particularly with very thin specimens.

Variations of the original Hopkinson apparatus have been used to study the high-rate properties of metals, rocks, plastics, cement, soil, and filled polymers. The technique has also been applied to various propellants and explosives by Murri et al. (1977), Hoge (1967), Hauser (1961), Fong (1985), James and Breithaupt (1984), Costantino and Ornellas (1987), and others.

Fong's primary interest was in determining the fracture behavior of gun propellant grains under impact conditions. Specifically, his objective was to detect the onset of fracture in multiperforated grains under

compressive loads using a variation of the Kolsky apparatus. An interesting feature of his work was the observation of "minor" and "major" yield regions on a load/displacement trace. These distinct regions were also resolved on graphs of load or stress as a function of projectile velocity. They may be interpreted as an elastic minor yielding and a major yielding due to crack propagation and/or plastic flow. A characteristic plot for seven-perforated grains is shown in Figure 1.

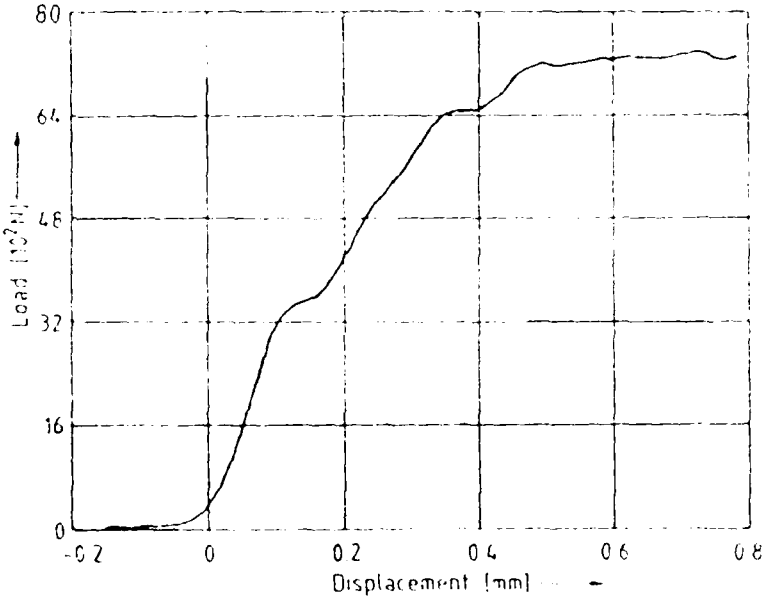

Figure 1. Load-displacement relationship for a single-base propellant grain.

Fong (1985) indicated that the minor yielding was possibly a result of both elastic deformation and minor

crack initiation. A scanning electron micrograph was used to observe the surface fracture pattern of impacted grains, and evidence of minor cracking was found around the center perforations of some of the grains. In addition, Fong reports that several minor yielding events were observable in test data, but that the observations were not consistent in every test. As a result, Fong applied a lower limit criterion to account for the random nature of crack initiation and propagation. A primary conclusion was that crack initiation may result in new surface areas available for combustion. Fong also indicated that friction between the new surfaces may produce hot spots and, therefore, ignition sites.

James and Breithaupt (1984) used the Hopkinson technique to evaluate the properties of several solid rocket propellant formulations. Initially, a compressive apparatus was used but was eventually replaced by a tensile version of the test due to data inconsistency when sample fracture did not occur. The samples were not perforated, as were gun propellant grains in the tests described above. The samples were also somewhat larger.

Stress/strain plots were generated for a number of formulations at various strain rates. Generally, the formulations tested were highly dependent on strain rate. Some of the plots show a "double hump" feature, reminiscent of the minor/major failures in Fong's experiments. The particle sizes of the solid-phase constituents were found to be particularly important in the load response characteristics observed.

The latter finding highlights a problem in the testing of composite materials like solid propellants. Sample size may affect the results, due to the fact that some of the constituent materials may be of relatively appreciable size compared to the size of the sample (see Marsh (1987) on size effects). The severity of this effect depends somewhat on the particle size of the oxidizer or fuel in the mixture. In addition, the propellant processing and sample fabrication steps may result in material defects or surface irregularities that may affect the results of a particular test. Propellants present a difficult challenge to the structural designer because the materials are generally difficult to characterize and are also relatively variable in their properties, as well as being anisotropic.

The effects of sudden application of load to explosive materials were studied by Hoge (1970). Responses to both tensile and compressive loads were evaluated at strain rates approaching 3,000/s. Generally, the composition of many explosive formulations is reasonably similar to that of a composite propellant. The mechanical properties of explosives, like solid propellants, are rate-sensitive, and this similarity extends to properties at high loading rates.

Several investigators have used other methods to determine response properties of energetic materials to high loading rates. Much of this work has been conducted by the U.S. Army at BRL and at the Large Caliber Weapons Laboratory, Picatinny Arsenal, New Jersey. As mentioned previously, much of this work has been done at lower rates of strain than can be obtained with a Hopkinson split-bar apparatus.

Lieb et al. (1981) used a drop weight tester to obtain stress/strain curves for a number of propellant formulations at strain rates up to about 300/s. Of primary interest was the determination of fracture strain values at various loading rates for fracture mechanics studies. Results for M30 are shown in Figures 2 and 3.

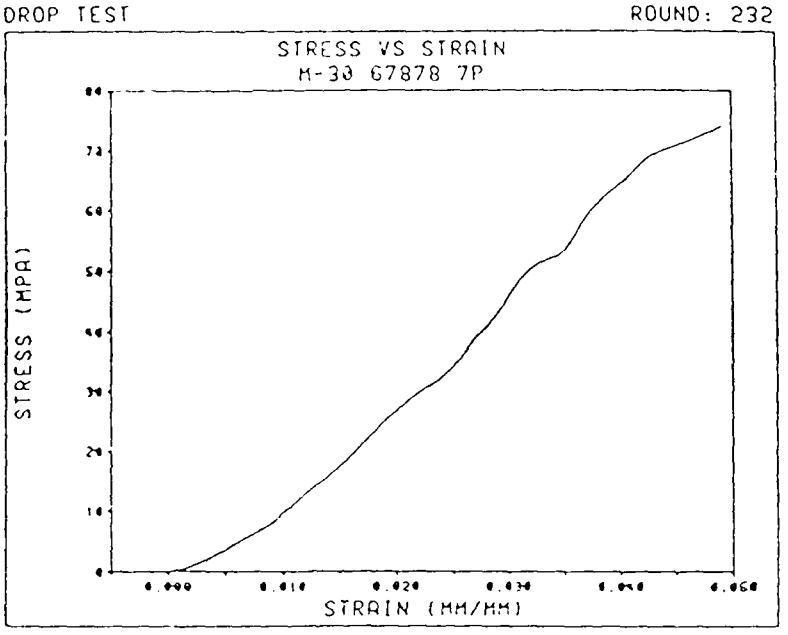

Figure 2. Stress versus strain for M30.

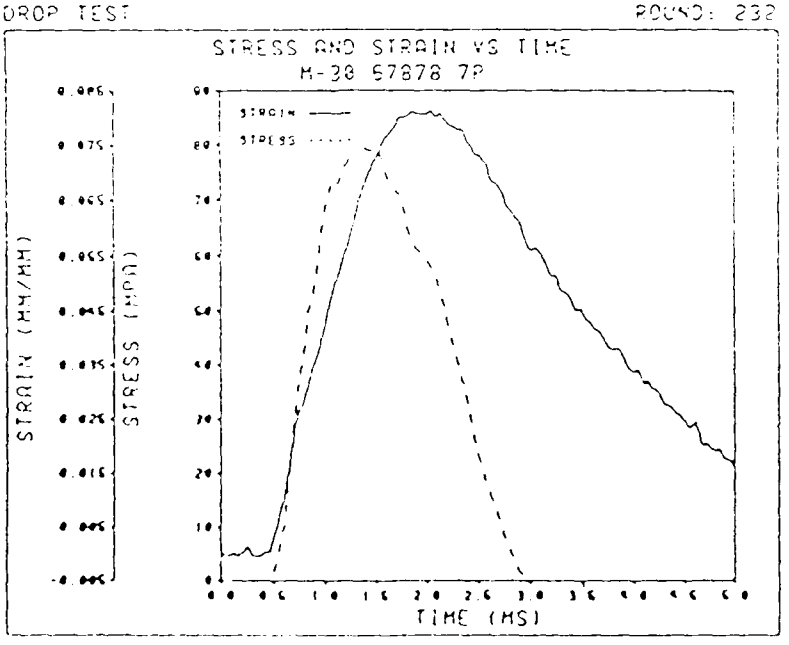

Figure 3. Stress and strain versus time for M30.

Costantino and Ornellas (1985 and 1987) obtained failure curves for the JA-2 and HELOVA (high energy/low vulnerability ammunition) propellants 1) under confinement at low rates and 2) under ambient pressures at much higher strain rates (up to 2,600/s). The confined tests were conducted under hydrostatic load with application of an additional axial load, resulting in a net shear loading. Their results for both JA-2 and HELOVA indicate a pressure effect on material strength, as well as a rate effect. Hydrostatic loads from 0.1 to 400 MPa (15 - 58,000 psi) were applied. Strain rates varied from 10^{-4} to 10^{3}/second at four levels. The material was driven to failure by low-rate axial loading superimposed on the hydrostatic load. The JA-2 tests indicated that the response was elasto-plastic: linear at strains of up to about 1% and nonlinear thereafter. The modulus determined for JA-2 was about 2.4 - 2.6 GPa at strain rates of about 1,500/second at ambient pressure. The resultant plots show maximum shear stress versus the log of strain rate is shown in Figures 4 and 5.

In earlier experiments at ambient pressure, Constantino and Ornellas (1985) determined the maximum stress values for HELOVA to be about 91 - 93 MPa at strain rates of

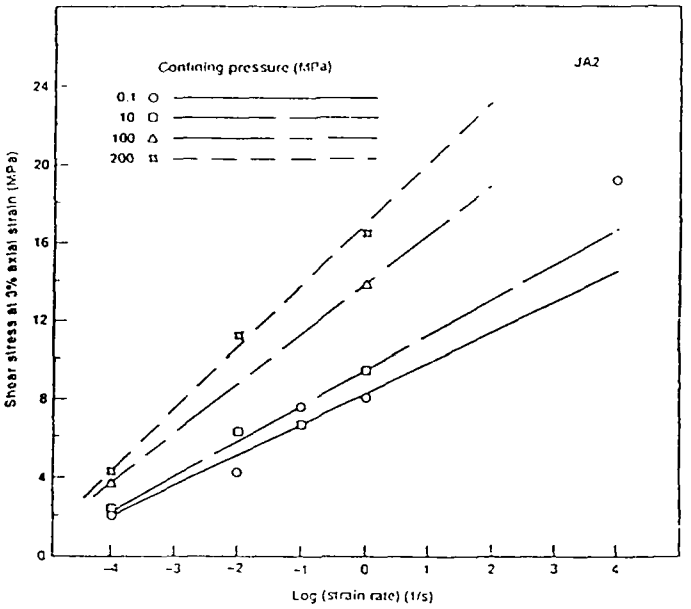

Figure 4. JA-2 strain rate dependence of axial stress.

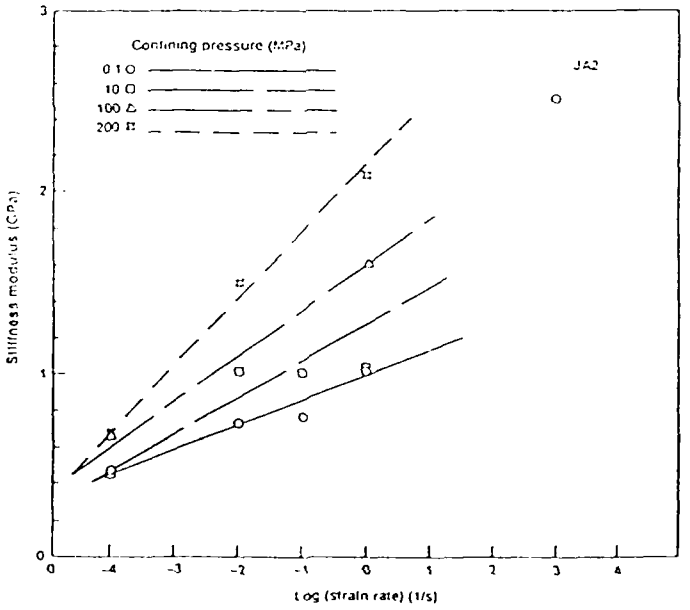

Figure 5. JA-2 initial modulus dependence on strain rate.

2,600/s. At an average strain rate of 1,600/s, the maximum stress was about 67 - 68 MPa.

The Hopkinson Split-Bar technique is used to determine characteristic material behavior outside the elastic range. A factor which complicates application of the technique to propellants is that generally propellants are viscoelastic materials whose exact properties are difficult to characterize. The most common approach to viscoelastic characterization is to determine linear constitutive equations based on time/temperature superposition. Unfortunately, the actual behavior of propellants is usually nonlinear, with memory effects.

Chapter 2

Experimental Apparatus

A summary of the theory for the Kolsky version of the Hopkinson split-bar or split-rail test is presented here. The Kolsky arrangement was used as the basis for both the ambient-pressure and high-pressure test devices.

Theory of Measurement

The basis for the Kolsky apparatus is a one-dimensional elastic wave theory. Pressure/time loading is applied at one end of an elastic bar of appreciable length. It is assumed that the suddenly applied loading will generate a wave in the elastic bar which propagates parallel to the longitudinal axis of the bar. If it is further assumed that the wavefront is planar, then a one-dimensional form of the wave equation may be applied. The fact that the loading is in the elastic range allows measurement of loads or displacements in the bar.

A typical test with the Kolsky apparatus occurs as follows: a compressive stress wave is initiated in a long elastic bar by means of an explosive percussion or by

impact from an incident projectile. If a projectile is used, the reflection of the compressive wave from the aft end of the striker unloads the bar and forms a pulse of finite length. The pulse wave propagates in the input bar longitudinally, and its amplitude is recorded as a function of time by strain gage instrumentation as it passes by the gage location. Ideally, the wave does not disperse during its travel. The wave then reaches the end surface of the input bar.

If a specimen is present, the wave is then partially transmitted and partially reflected. The reflected portion is directly proportional to the rate of strain in the specimen, as will be explained in a later section. The portion of the pulse that is transmitted into the specimen reflects off of the ends of the input and output bars many times. The exact nature of the interaction depends on the geometry of the specimen and the relative impedance mismatch between the bar material and the specimen.

For a compressive strain wave induced in an elastic rod, interaction with the free surface at the rod end produces a reflected tensile wave and a transmitted compressive wave. The magnitudes of the transmitted and

reflected waves are dependent on the properties of the specimen sandwiched between the pressure bars, specifically its characteristic impedance. The impedance of a material to the transmission of a wave was described by Davies and Hunter (1963) and by Hoge (1970). Impedance is defined as $Z = A(\rho E)^{1/2}$, where A is the area, ρ is the density, and E is the Young's modulus of the material. The mismatch in the impedances of the input bar and specimen determines the relative transmission properties of the pulse.

The transmitted pulse begins to load the specimen by reflecting through the length of the material. The rate of loading is somewhat dependent on the length of the specimen and on the end conditions of the specimen. The end conditions are important because if there is friction between the end of the bar and the face of the specimen, radial deformation will be retarded and apparent stresses will result. Inertial forces may also result in apparent stresses. It is assumed that the specimen is in equilibrium when the stress state through the length of the specimen is uniform. That a finite period of time is necessary to reach equilibrium means that, for many materials, the initial portion of a graph of stress as a function of strain may not be meaningful. However, Davies

and Hunter (1963) found that the point at which the specimen reaches stress equilibrium may be determined from a stress-strain graph using the following criterion:

$$\frac{d\sigma}{d\epsilon} > \frac{\pi^2 \rho_s l^2}{T^2} .$$

This criterion may be used to determine that the viscoelastic samples under consideration in this study equilibrate rapidly. Therefore, the stress-strain curves may be used to determine an effective modulus. Davies and Hunter (1963) evaluated the response properties of various polymeric substances to high strain rates with this approach. They determined that the limiting high frequency behavior of a viscoelastic material could be assumed to be linear, and that an initial modulus could be determined for the viscoelastic materials in a "glassy" state, analogous to elastic behavior.

The theory of one-dimensional wave propagation in elastic media is well developed and readily applicable. A summary of the theory follows, derived mainly from Kolsky (1963).

A small element of cylindrical bar with thickness dx and cross sectional area A is subjected to a stress wave, of magnitude σ. The stress on one face is σ while the

stress on the other face is $\sigma + (\partial\sigma/\partial x)dx$. The components of Newton's second law of motion (F=ma) may be written for the element:

$$F = [\sigma + \frac{\partial\sigma}{\partial x} dx - \sigma] A$$

$$F = \frac{\partial\sigma}{\partial x} dx\ A = ma,$$

$m = \rho\ A\ dx$, $a = \frac{\partial^2 U}{\partial t^2}$. Assembling these, $\frac{\partial\sigma}{\partial x} = \rho \frac{\partial^2 U}{\partial t^2}$.

For isotropic elastic materials, $\sigma = E\epsilon$, where $\epsilon = \partial U/\partial x$. The partial derivative of Hooke's law with respect to x is

$$\frac{\partial\sigma}{\partial x} = E \frac{\partial^2 U}{\partial x^2} .$$

Substituting $C_0^2 = E/\rho$ results in an expression for the propagation of a longitudinal wave :

$$\frac{\partial^2 U}{\partial t^2} = C_0{}^2 \frac{\partial^2 U}{\partial x^2} .$$

A harmonic wave may be assumed. Taking the partial derivatives of u with respect first to x and then to t,

$$\frac{\partial U}{\partial t} = C_0 \frac{\partial U}{\partial x} = C_0 \frac{\sigma}{E} .$$

This reduces to $\sigma = \rho\ C_0 v$, where v is particle velocity.

If the incident, or input, bar has a stress wave propagating through it, the particle velocity associated with the wave front is $v_i = \sigma_i/\rho C_0$. The impedance difference between the specimen and the bar material result in a partial propagation of the wave. Part of the wave is reflected as a tensile wave. If the interface between the incident bar and the specimen is labeled interface 1, and that between the specimen and the output bar as interface 2, then $v_1 = v_i - (-v_r)$, and $v_2 = v_t$ (Figure 6). The difference between the particle velocities at the interfaces gives the strain rate in the sample. Therefore, the amplitude of the reflected wave is proportional to the strain rate in the sample. Integrating the strain rate gives the strain in the sample:

$$\epsilon = \int_0^t \epsilon \, dt \ .$$

The velocity/stress relation may be used to calibrate the strain sensing and recording devices used in the system.

The importance of the length-to-diameter ratio of the specimen has been evaluated (Bertolf and Karnes, 1974) relative to interface friction and specimen load equilibrium. Davies (1948) found that a length-to-

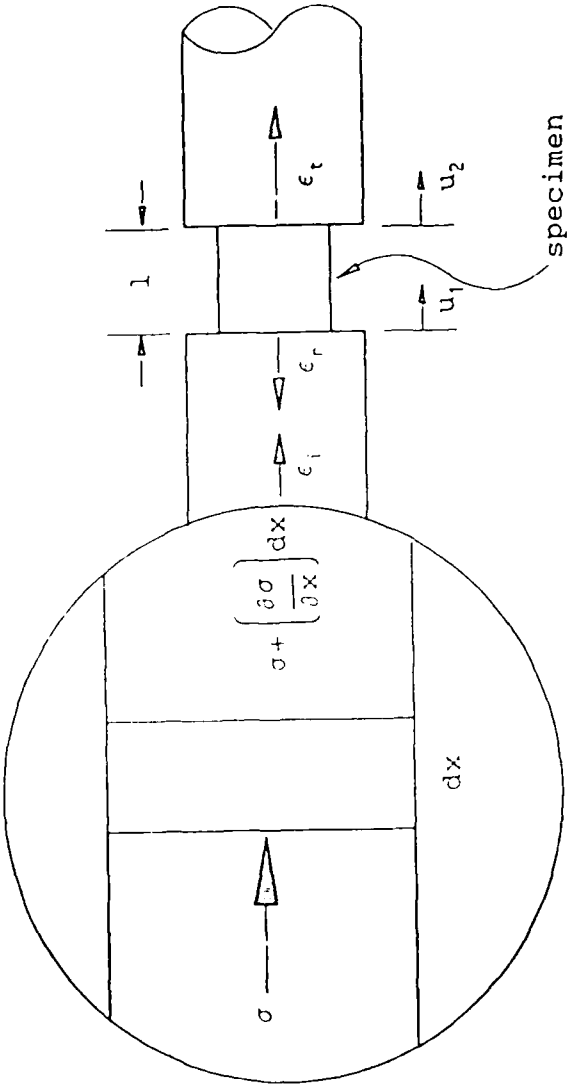

Figure 6. Stress wave transmission through a bar and specimen.

diameter ratio of unity was desirable to accommodate both of these considerations simultaneously.

Ambient Pressure Apparatus

The apparatus used in the current study basically consists of a set of elastic bars, a table with adjustable alignment mounts for the bars, a gas gun and striker projectile for initiating an elastic pulse in the bars, and a system for recording the history of the reflected wave in the input bar and the transmitted stress wave in the output bar (strain gages and signal conditioning units). The specimen is sandwiched between the two pressure bars (see Figure 7).

At the University of Maryland, both steel and aluminum pressure bars were used. The strains were detected with 1,000-ohm gages paired on the bars to eliminate the effects of bending: only the plane strain wavefront was to be recorded. Aluminum bars were used to improve the signal-to-noise characteristics of the apparatus by matching the impedance of the elastic bar to the gun propellant more closely. The ½-inch-diameter aluminum rods were each 1.2m (4 ft.) long, with strain gages placed approximately in the center of the lengths. The striker was of the same material as the bars.

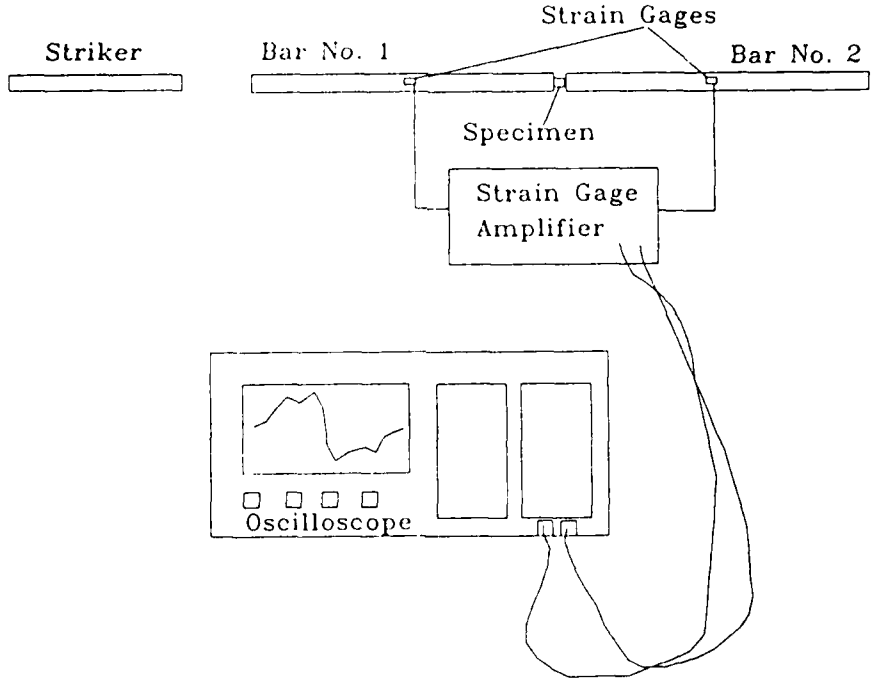

Figure 7. Arrangement of the ambient pressure test apparatus.

The strain gage bridges were powered and their signals were output by MicroMeasurements' BAM-1B bridge circuits. The frequency response of these units ranges from 0 to 120 kHz, adequate capacity for good signal representation. A Nicolet digitizing oscilloscope was used to record and to view the strain gage signals. The time base used in the tests ranged from 500 nanoseconds to 2 microseconds per data point. The features of the instrumentation allowed very precise records of the strain histories for the input and output bars to be stored and resurrected for later manipulation. Data was stored on the Nicolet's bubble memory and transferred to floppy disk storage as ASCII files. A personal computer was used with commercially available spreadsheet software (LOTUS ^{tm}) to reduce the data and to prepare graphs.

The experimental setup for ambient pressure tests at the BRL-IBD was much the same as that at the University of Maryland. The bars used were aluminum, 12.7-mm (½-inch) diameter and 1.2m (4 ft.) long with 1,000-ohm bridge gages. The gas gun used was also similar; 0.15m- and 0.23m-long (6- and 9-inch) striker slugs were used. The bridge circuits were powered by MicroMeasurements' 2310 Signal Conditioning units. Conditioned signals were input to a Norland 3001/3001A Processing Digital Oscilloscope.

Velocity/pressure profiles were generated for the gun to allow some control over striker velocities and the resultant strain amplitudes and rise times.

High-Pressure Device

The high-pressure Hopkinson split-pressure bar device was designed to simulate the pressure regime present in the gun chamber during the ballistic cycle. The device was designed to be pressurized to about 200 MPa (30,000 psi) with a factor of safety of about 5 for most components. A schematic for the device is shown in Figure 8 with details of the assembly in Figure 9. Basically, it consists of a Hopkinson split-pressure bar apparatus contained in a pressure vessel, and a pressurization system.

Other high-pressure adaptations of the Hopkinson split-bar have been devised. The present design is similar to a device built at the University of Utah by Christensen et al. (1972). Chalupnik and Ripperger (1966) also developed a high-pressure application of the Kolsky apparatus.

The device is comprised of a pressure vessel, aluminum bars, closure plugs, bar alignment rings, a

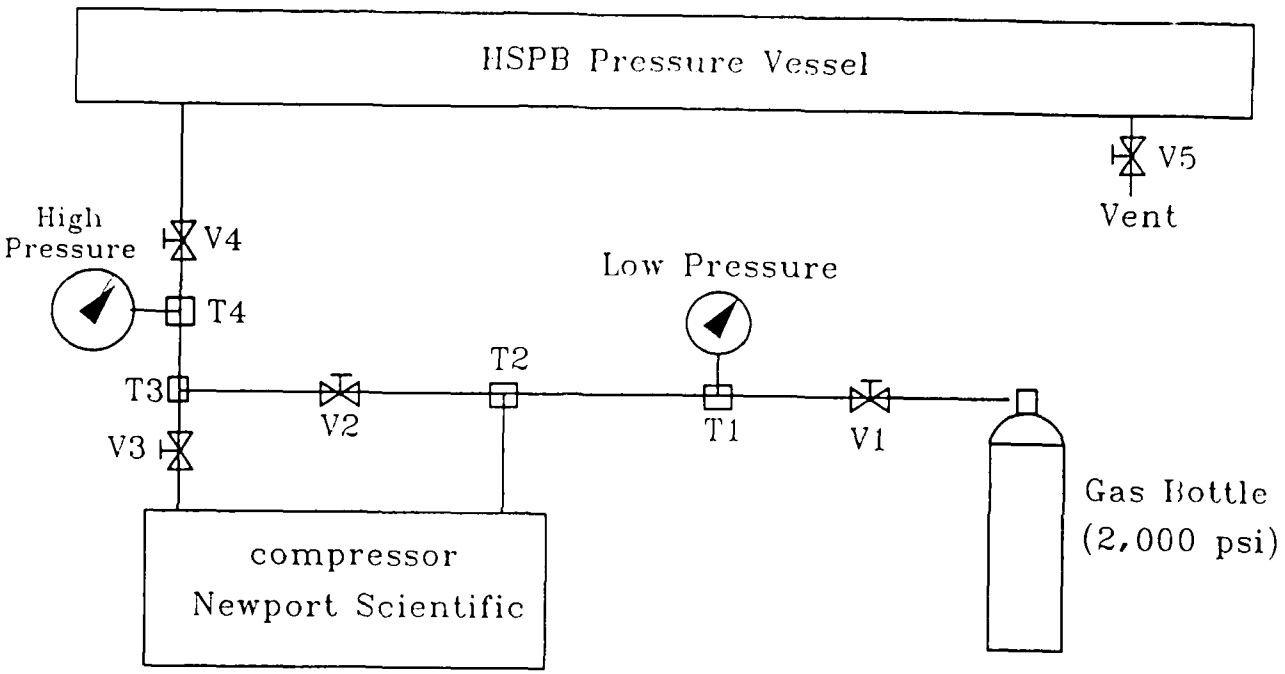

Pressured Hopkinson Split-Bar Layout Schematic
Basic Pressurization System

⋈ = Valve

Figure 8. Pressurization System for HSPB Testing.

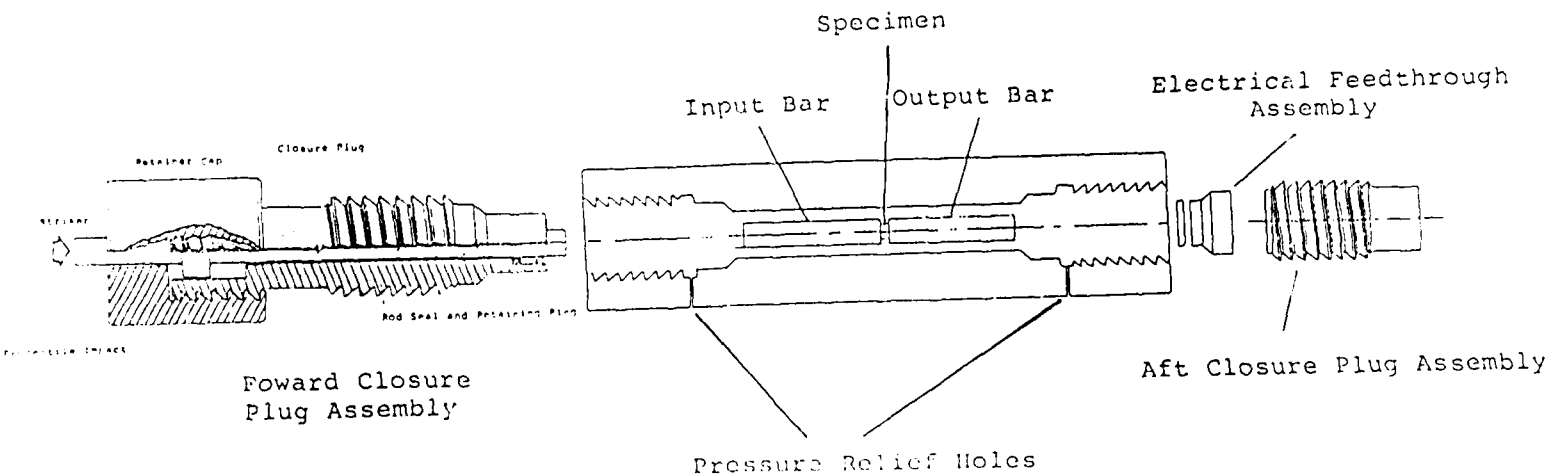

Figure 9. High-Pressure HSPB Vessel Component Assembly.

pressurization system, striker, and instrumentation. The forward closure plug contains a striker, which transmits the stress wave into the pressure vessel and initiates the stress wave in the input bar. Details of the component designs and basic calculations are contained in the Appendix.

The pressure vessel was designed around an available Mann barrel (a type of smoothbore gun barrel often used in testing) fabricated from SAE 4340 steel. The barrel was 1.8m (6 ft.) long, allowing the use of pressure bars up to almost 0.9m (3 ft.) long. Aluminum bars and striker were specified, again to more closely match the impedance of the propellant samples to be tested.

The design allows for a gaseous pressurant, as opposed to a liquid. The primary reasons for the selection of a gaseous pressurant are 1) the desire to closely simulate the combustion gases in a gun barrel, and 2) the potential for improved ease of use over liquid pressurants, as the system will require access to the barrel interior and to the test specimen for each test. The selection of a gaseous pressurant necessitated application of rigorous design safety margins and safety procedures during use.

A Newport Scientific Double End Compressor was selected as the pressurizing device. The system was specially manufactured to allow pressurization to 200 MPa (30,000 psi) using a 14 MPa (2,000 psi) nitrogen supply. About 2 hour's time is required for the pressurization cycle for each test.

Chapter 3

Strain-Rate Dependence of Materials

The materials characterized in this study, all gun propellant formulations or inert simulants, were JA-2, M30, and HELOVA. The M30 and JA-2 formulations consist of nitrocellulose, nitroglycerin, and nitroguanidine. The JA-2 propellant also contains an energetic plasticizer, diethyleneglycoldinitrate (DEGDN), to improve performance. The HELOVA propellants include a nitramine oxidizer, RDX, and a polymeric binder. The formulations may be characterized as viscoelastic materials, i.e., their properties are dependent on strain rate and temperature. In addition, the solvent content of the propellant formulations may vary over a fairly wide range, resulting in varying properties as a result.

Data Recording and Reduction

Each test produced two strain-time traces to be analyzed. The first is a record of the strain in the input bar due to the passage of the strain pulse. A typical strain-time history for the input bar (HELOVA

propellant) is shown in Figure 10. As mentioned above, the strain pulse history starts with a compressive wave, which results from the impact of the striker slug on the end of the bar and, after a few microseconds delay, a tensile wave reflected off the aft end of the striker unloads the bar. Alignment and surface conditions are critical to the resulting shape of the pulse.

The pulse travels past the strain gage, producing the initial part of the trace. The next part is a reflected tensile wave, due to the interaction between the pulse and the specimen/bar-end interface. The reflected pulse is directly proportional to the rate of strain versus time in the specimen and may be integrated to find the strain at any point in time. Conversely, if no specimen is present, and with perfect alignment and end conditions, the initial compressive wave should be transmitted into the output bar with no reflection, and no change in shape. For this reason, calibration shots may be conducted without specimens to determine if the system is properly aligned. Similarly, the strain transmitted into the output bar (Figure 11) is proportional to the stress in the sample. A Lagrangian diagram for the event is shown in Figure 12.

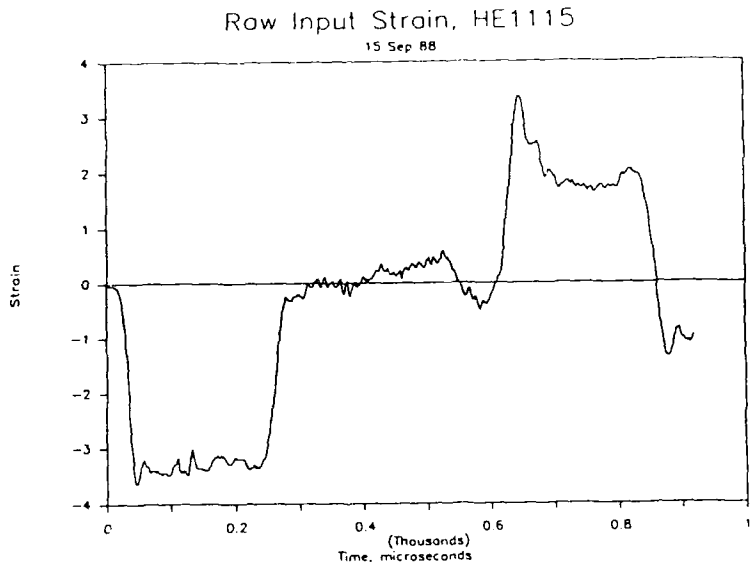

Figure 10. Input bar strain-time history.

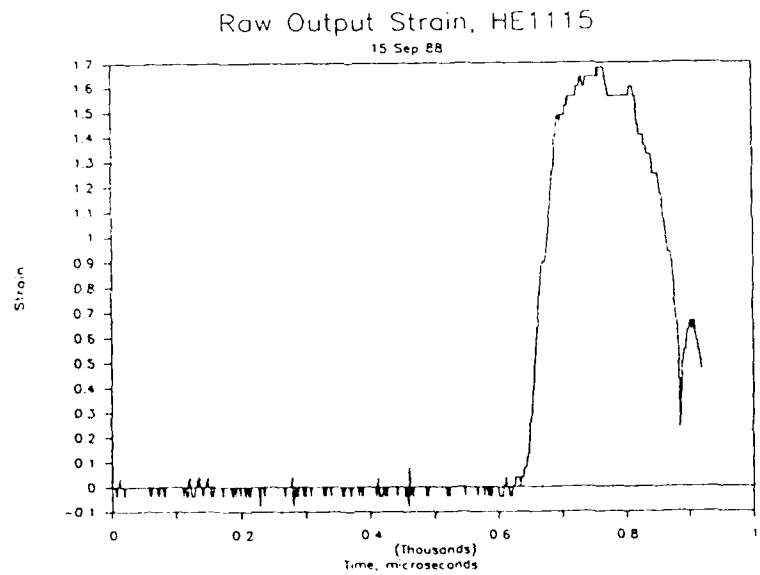

Figure 11. Output bar strain-time history.

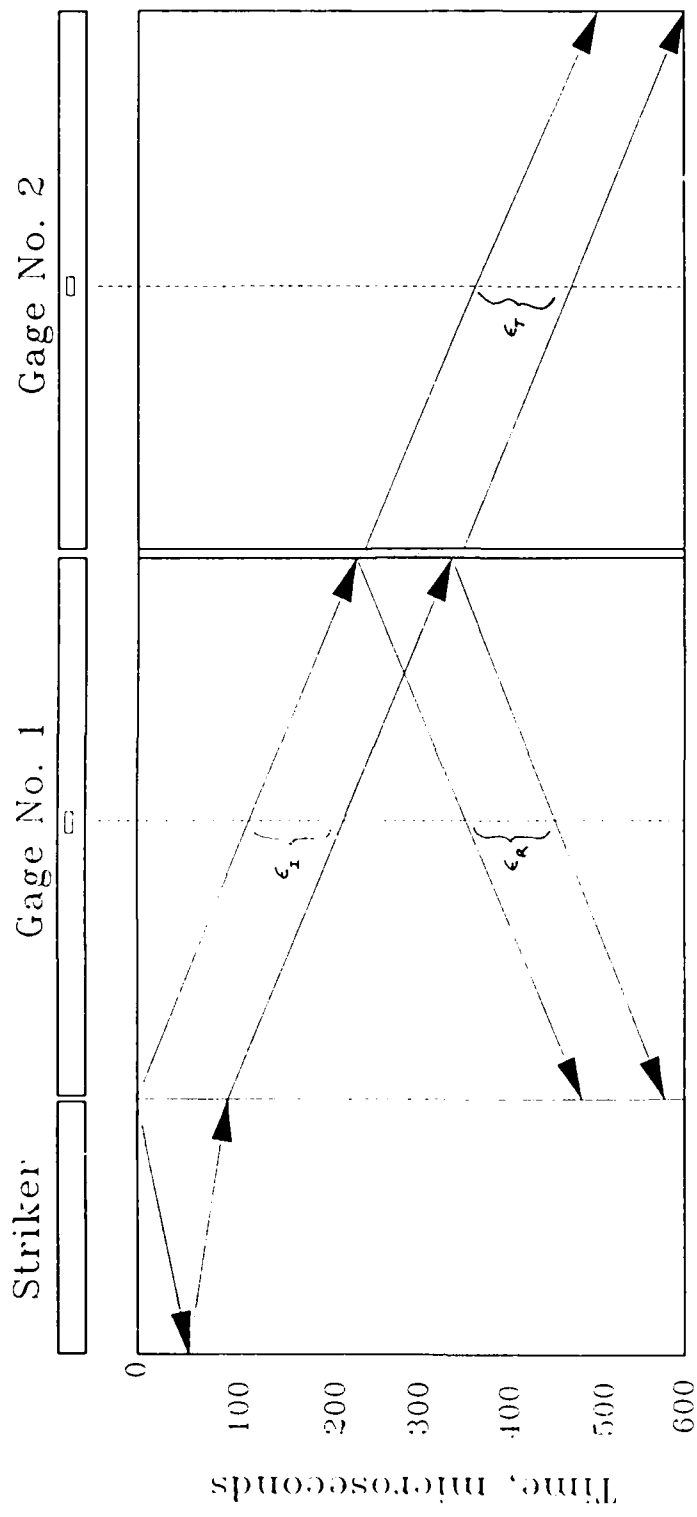

Figure 12. Lagrangian Diagram for the Ambient Pressure HSPB.

From each test three measurements are obtained: sample stress from the output bar and sample strain rate from the input bar are recorded directly as a function of time. Sample strain as a function of time is obtained from integration of the strain-rate history. The stress-time and strain-time histories may then be used to create a stress strain plot.

Discussion of Results

A typical data reduction procedure is presented for the HELOVA propellants. The raw input bar pulse amplitudes are directly proportional to the magnitude of the strain rate in the sample, which is shown in (Figure 13) as a function of time. The output bar strain history is directly proportional to sample stress as a function of time (Figure 14). Cross plotting the stress and strain histories results in the stress-strain curve (Figure 15). The point at which the sample reaches equilibrium was estimated using the method of Davies and Hunter (1963). An effective modulus was estimated from the initial linear portion of the graph.

Test parameters and calculated results are presented in Table 1, including stress, strain and effective

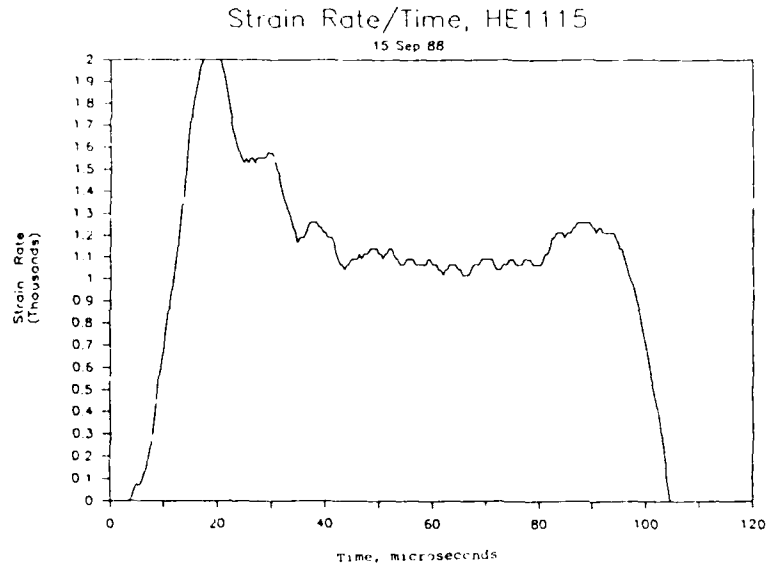

Figure 13. Strain rate versus time for test HE1115.

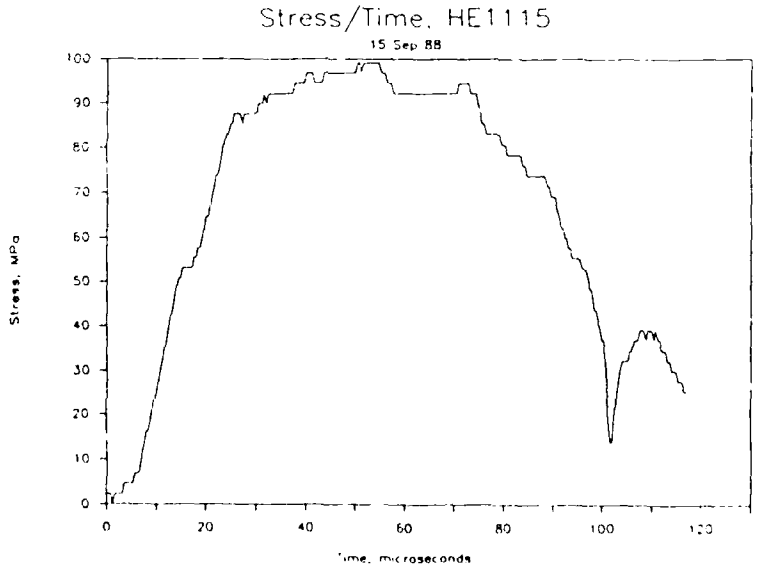

Figure 14. Stress versus time for test HE1115.

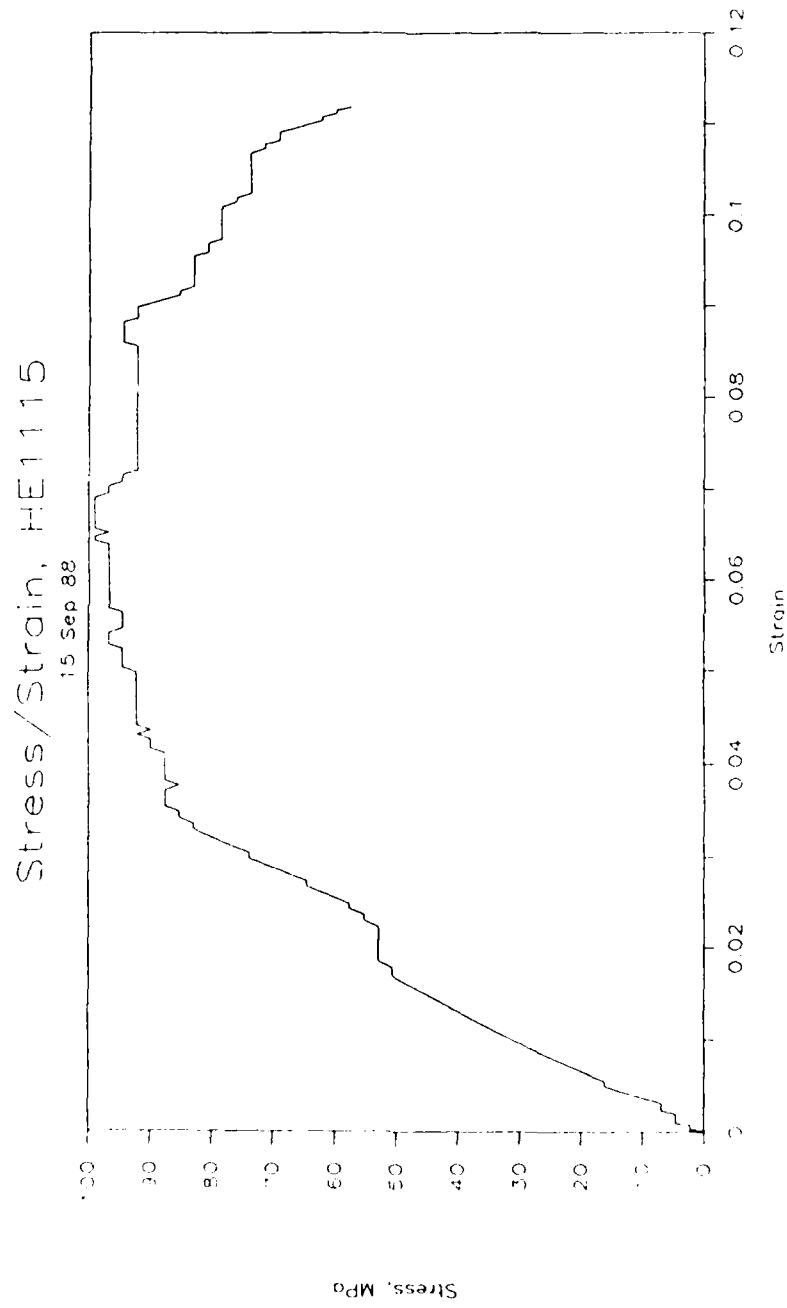

Figure 15. Stress-strain curve for test HE1115.

Table 1. Test parameters and results for ambient pressure HSPB

Test ID	Diameter mm	Length mm	Maximum Stress MPa	Strain Rate	Effective Modulus GPa	Yield Stress MPa
HE1015	9.5	8.9	93	936	4.88	50
HE1115	9.6	7.8	97	1,097	3.03	53
HE315	9.3	8.5	105	1,368	8.18	70
HE415	11.4	8.0				
HE515	11.3	9.8	85	1,027	4.9	47
HE614	10.5	11.7	44	620	2.14	25
HE615	9.6	9.5	47.5	621	1.96	23.5
HE714	10.6	8.3	43	740	1.96	15
HE715	9.6	9.5				
HE814	10.7	8.4	48	755	1.08	
HE815	9.1	7.8	95	1,414	5.88	48
HE914	10.8	11.4	45	808	1.92	28
HE915	9.2	8.9				
JA22701	8.6	9.2	27	1,207	2.376	22
JA22704	8.7	8.5	25.8	1,308	1.715	21
JA22705	8.7	8.0	27.2	1,357	2.6	21.55
JA2276	8.9	8.8	27	1,408	3	21.5
JA2277	8.8	9.5	26	1,286	2.73	22.8
JA2311	8.6	9.2	29	1,190	2.73	22
JA2312	8.6	9.2	33	1,442	2.353	27
JA2313	8.8	7.7	34	1,050	3.07	17
JA2315	8.6	9.2	26	1,416	2.154	21.5
JA2316	8.6	9.2	31	1,429	2.06	23
JA251	8.7	7.7				
JA252	7.1	7.8				
M302708	7.0	5.9				
M302711	7.8	7.4				
M30317	7.1	9.1	91	1,126	1.09	
M30318	7.1	6.9	97	1,552	1.35	
M3053	7.1	7.0	93	1,698	1.496	
M3054	7.1	7.4	93	1,468	1.2	
M3055	7.0	6.2	100	1,680	1.25	
M3056	7.0	6.4	105	1,574	1.18	
M3057	7.0	7.6	95	1,365	1.32	
M3058	7.1	7.8	91	1,333	1.03	
M3061	7.1	7.4	107	1,315		
M3062	6.1	8.7				
M3064	7.0	8.6				
M3065	7.1	8.8				

modulus. Values of maximum stress were determined from the stress/strain plots.

JA-2 Propellant Results

JA-2 is a much softer material than either M30 or HELOVA. This fact can be seen in the unreduced data traces for the HSPB tests, where the output strains with JA-2 samples are quite low relative to those from tests with M30 or HELOVA. The graphs are not corrected for changes in cross-sectional area, so that the actual or true stress/strain graphs may not have the same features.

JA-2 yielding occurred on average at strains of about 1%, under strain rates of 1,500/s. The "yield stress" was observed at about 20 - 22 MPa, followed by a plastic zone to failure, which occurred at about 28 - 32 MPa. The initial elastic modulus, as indicated in the stress strain curves, was about 2.0 - 2.5 GPa.

The shape of the stress strain curves obtained for JA-2 is generally repeated in the results for most of the tests. The curves seem to indicate a linear region of high modulus at low strain, followed by a "yield point" to a region of lower modulus. The elastic-like region obtains to strains of about 1.0 - 1.5%. Since most of

the tests were conducted at strain rates of 1,200 - 1,500/s, it is not surprising that the "yield point" stresses and maximum stress values are fairly consistent. The results of the preliminary tests on the JA-2 propellant seem to confirm the earlier results of Costantino and Ornellas (1987), in terms of modulus and maximum stress, for tests conducted in the same strain-rate regime. Costantino and Ornellas' data are somewhat more consistent (the scatter in the current data may be seen in Figures 16, 17, 18, and 19). A graph of maximum stress versus strain rate, incorporating data from Lieb et al. (1981) and from Costantino and Ornellas (1987), as well as data from the current study, indicates a slight dependence of stress versus strain rate. A stronger dependence of modulus on strain rate may be seen in the data.

M30 Propellant Results

Maximum grain stresses ranged from about 95 to 105 MPa; strains at maximum stress averaged approximately 8%. The strain rates for the initial series of tests ranged from about 1,500/s to 1,900/s. Further data reduction, to account for area changes, may be needed.

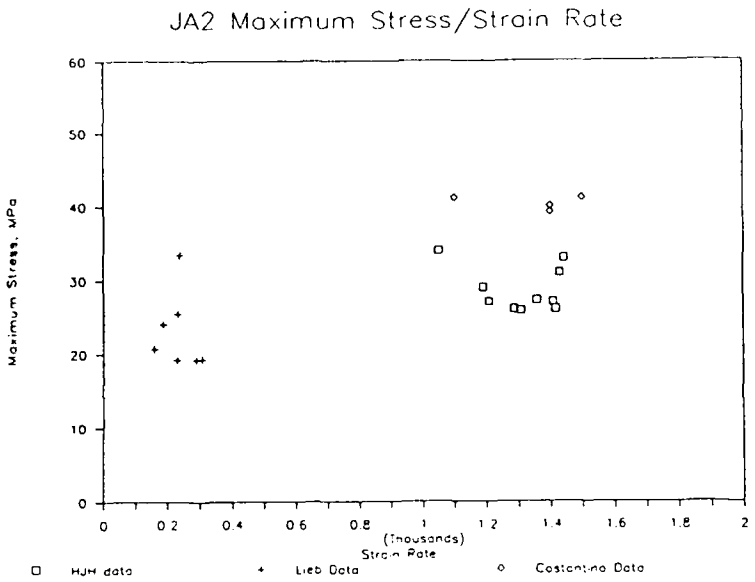

Figure 16. JA-2 stress dependence on strain rate.

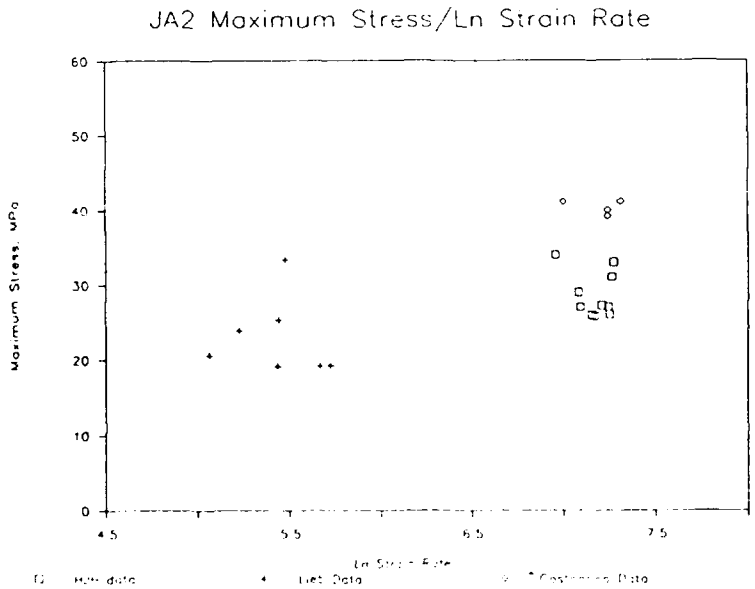

Figure 17. JA-2 effective modulus dependence on strain rate.

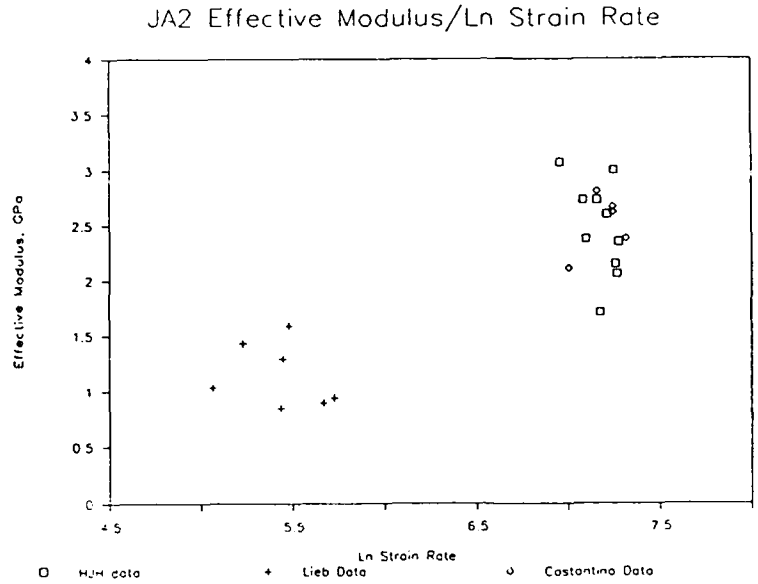

Figure 18. JA-2 effective modulus dependence on log strain rate.

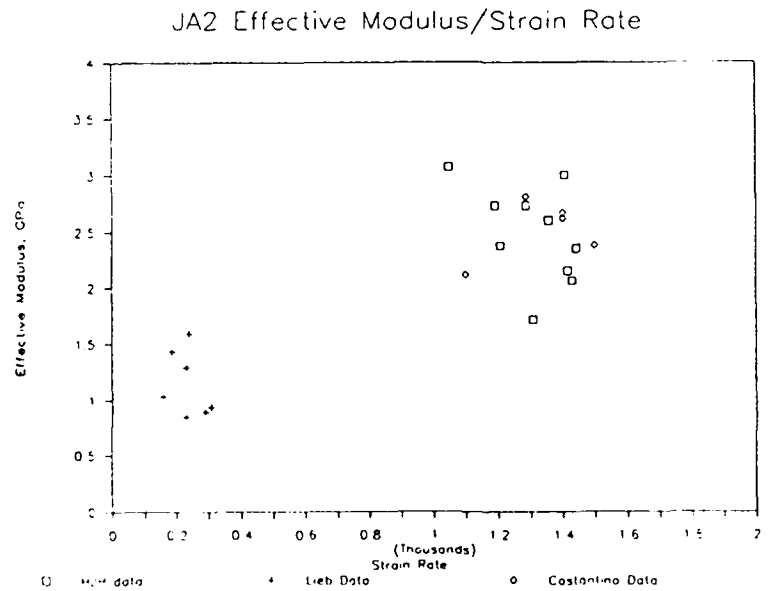

Figure 19. JA-2 dependence of maximum stress on log strain rate.

These results contrast somewhat from the earlier results of Lieb et al. (1985), at much lower strain rates. They reported failure stresses of about 115 MPa, at strains of about 5% under strain rates of about 300/s. An effective modulus for M30 was reported at about 4.7 GPa at those strain rates. Wires et al. (1979), also reported much higher moduli for lower rate tests with M30. They determined the average elastic modulus for M30 at strain rates from 67/s to 100/s to be 1.90 GPa; M30 maximum stress averaged 75.9 MPa.

The large discrepancies with the earlier results will require extensive evaluation and additional testing in order to determine if experimental artifacts are manifested in the current results. Great difficulty was encountered in determining the effective modulus from the stress/strain graphs, due to the fact that a linear region was often not apparent. A particular experimental problem with M30 was the fact that it was very difficult to obtain grains that could be cut to produce uniform right-circular specimen cylinders. Many of the specimens had some curvature. The degree to which this factor affected the results is not known.

Graphs of M30 maximum stress and effective modulus as functions of strain rate indicate a slight dependence for both properties on strain rate (Figures 20, 21, 22, and 23). Although there is significant scatter in the data, a definite increase in stiffness may be observed.

HELOVA Propellant Results

Only a very small number of tests with HELOVA were successful. Results for HELOVA tests were affected by instrumentation failures to some degree. The output bar traces showed particularly strong digitization effects, limiting the usefulness of the resultant stress strain plots. Nevertheless, the data were used to determine values for effective elastic moduli, maximum stress, and "yield stress" as a function of strain rate, and the natural log of strain rate.

Plots of modulus and maximum stress as a function of strain rate are shown in Figures 24 and 25. Once again, as with the other two types of propellants tested, a strain rate effect may be observed. Test parameters were varied to produce strain rates ranging from 620/s to 1,400/s.

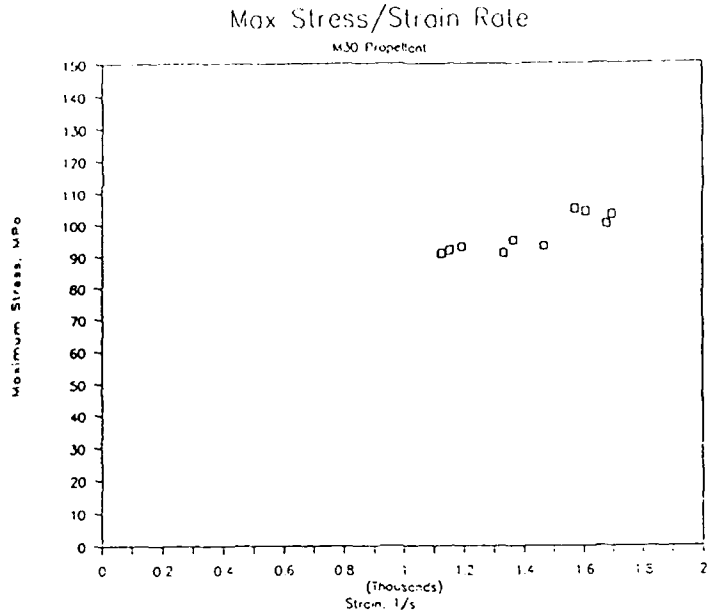

Figure 20. M30 maximum stress dependence on strain rate.

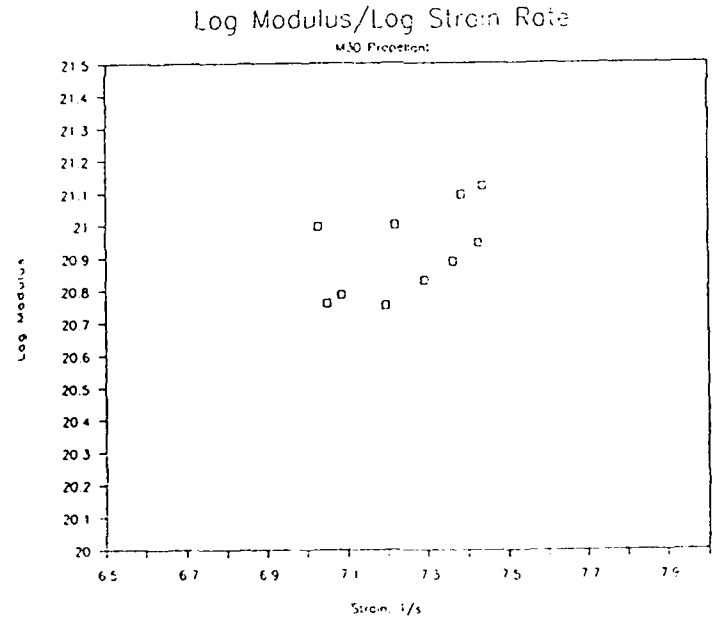

Figure 21. M30 effective modulus dependence on strain rate.

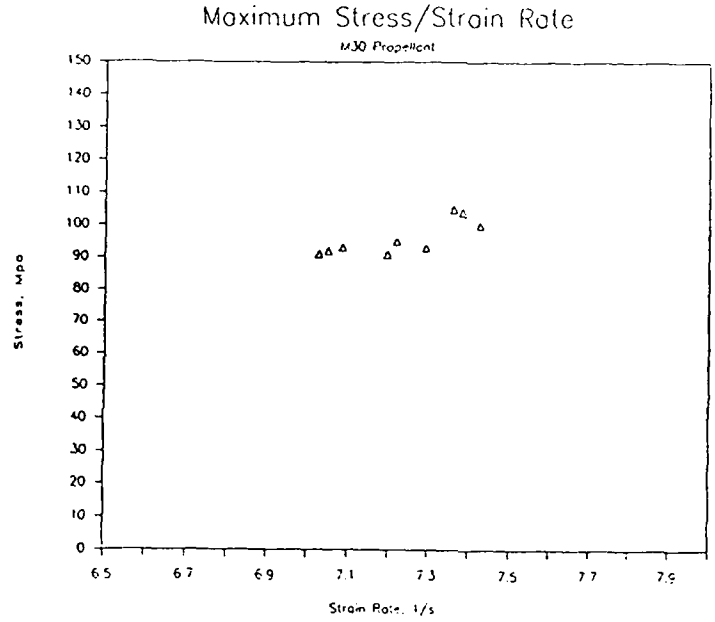

Figure 22. M30 maximum stress dependence on log strain rate.

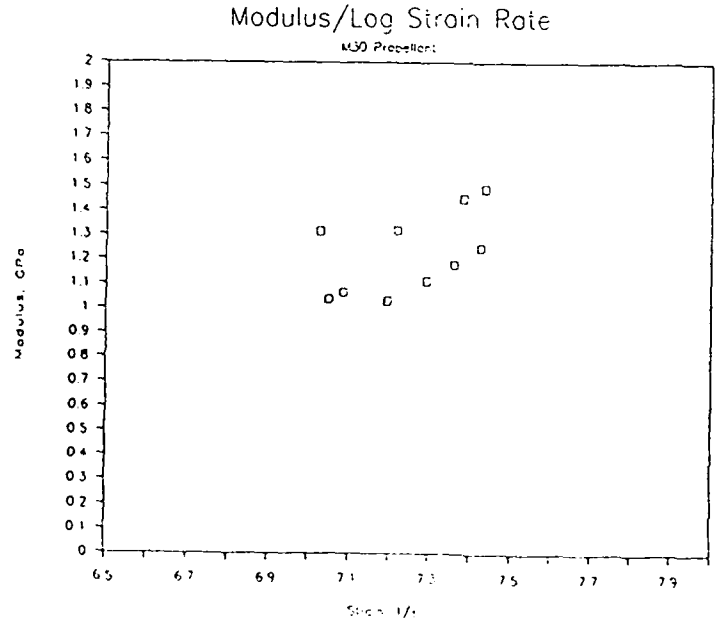

Figure 23. M30 effective modulus dependence on log strain rate.

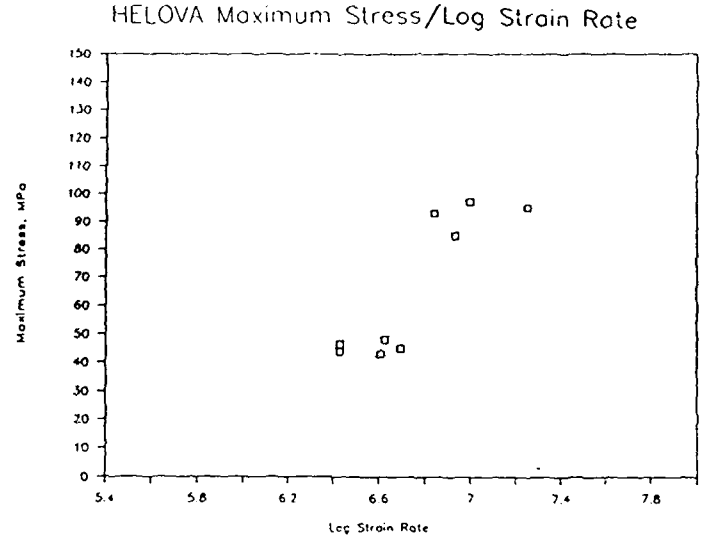

Figure 24. HELOVA stress dependence on strain rate.

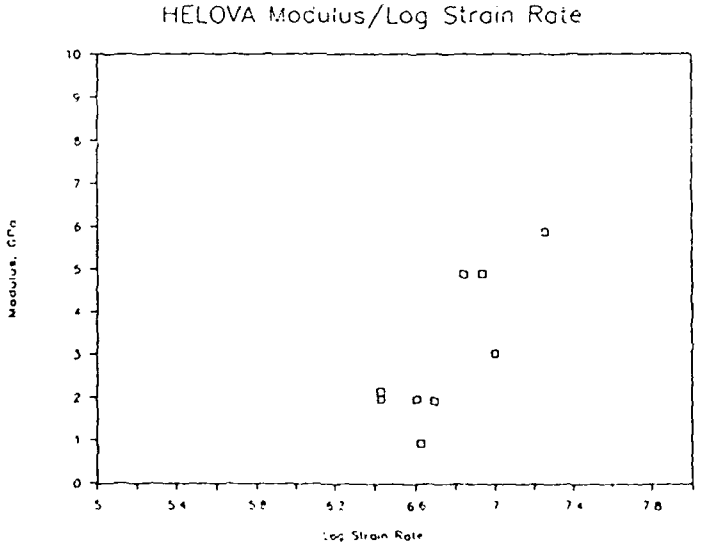

Figure 25. HELOVA modulus dependence on strain rate.

Effective elastic modulus ranged from about 1.8 GPa to 8 GPa over a rate range of about 600/s - 1,400/s. Yield stress values indicated a similar trend, ranging from about 40 MPa to about 95 MPa.

Costantino and Ornellas' (1985) LOVA data indicate somewhat lower stress values at higher strain rates under ambient pressure (moduli were not reported). However, the increase in maximum shear stress with strain rate shows a strong strain-rate dependence. Alternatively, Lieb and Rocchio's (1982) tests on HELOVA at lower strain rates (250/s) resulted in higher stress and modulus values.

Chapter 4

Conclusions

A Hopkinson split-bar apparatus was designed and constructed at the U.S. Army's BRL. Preliminary tests were conducted on three types of gun propellants to determine the high-strain rate response characteristics of the materials.

A pressurized version of the Hopkinson split-bar apparatus was designed to permit testing of materials under hydrostatic loadings of up to 200 Mpa (30 ksi) at high-strain rates. Fabrication of the component parts is underway at the BRL. Commercially available components have been ordered. A procedure was devised for testing with the high-pressure equipment.

Prelimary tests conducted on the JA-2 propellant resulted in mechanical properties that agree closely with reported data. Although the amount of data is limited, a definite effect of strain rate is apparent in the results. A much more extensive characterization program will be

required in order to develop a viscoelastic model for use in a finite element code.

Data collected for M30 are, however, somewhat problematical. Although the values determined for stress as a function of strain rate seem to agree with earlier data, values obtained for the effective elastic modulus do not. The tests were conducted at higher rates than have been reported in the literature, but values for the elastic modulus were much lower. Problems with test techniques may have contributed to the apparent discrepancies with existing results. Further, more complete work is required in this area.

Although only limited amounts of valid data were collected, results for HELOVA also tend to confirm trends seen in earlier work by other researchers. The data seem to clearly show a strong dependence of response properties on strain rate.

In general, there is not much information available concerning the properties of gun propellants at very high-strain rates. The limited data that exist for the three propellant types evaluated show dependence on loading rate to varying degrees. A much more complete characterization

effort is required to develop quantitative constitutive equations for the materials.

Appendix

Pressurized HSPB Device Design

The primary design concerns involved in the development of the pressurized HSPB device were the pressure vessel and its component parts. Given that the design was developed around an available steel gun barrel, the primary drive was to maximize the margin of safety for the complete pressure vessel.

The Mann barrel was fabricated from SAE 4340 steel, heat treated to give a Brinnel hardness of 283, corresponding to Rockwell C hardness 31. The hardness of the steel was determined by personnel at the U.S. Army BRL. The approximate yield stress corresponding to the measured hardness is 862 MPa (125,000 psi) with an ultimate stress of 1.00 GPa (145,000 psi) (see Baumeister et al. (1979)). The yield stress value was used in safety factor calculations.

The calculations for the stress state of the barrel were made using standard stress formulas for a thick-walled cylinder (Timoshenko and Goodier (1970)).

The calculations for the stress state of the barrel were made using standard stress formulas for a thick-walled cylinder (Timoshenko and Goodier (1970):

$$\sigma_t = \frac{a^2 p}{b^2 - a^2}\left(1 + \frac{b^2}{r^2}\right) \quad ; \quad \sigma_{tmax} = p\,\frac{b^2 + a^2}{b^2 - a^2}$$

$$\sigma_r = \frac{a^2 p}{b^2 - a^2}\left(1 - \frac{b^2}{r^2}\right) \quad ; \quad \sigma_{rmax} = -p_i\,\frac{b^2 - a^2}{b^2 - a^2}$$

$$\sigma_l = \frac{p\,a^2}{b^2 - a^2} \; .$$

A distortion energy approach was determined to be an acceptable failure criterion for the resultant triaxial stress state:

$$2\,\sigma_y^2 = (\sigma_1 - \sigma_2)^2 + (\sigma_2 - \sigma_3)^2 + (\sigma_3 - \sigma_1)^2 .$$

$$\sigma_y^2 = 3.797\,p^2 \quad : \quad p_i \approx 440 \text{ MPa } (64{,}000 \text{ psi}) \; .$$

Plastic analysis applied to the pressure vessel gives a somewhat larger margin of safety. Very high quality surface finishes on the interior and exterior portions of the vessel were specified, to eliminate stress concentrations that might reduce the factor of safety to unacceptable levels.

The closure plugs for the Mann barrel were designed to seal the pressure vessel and to reduce the effects of

the triaxial stress state resulting from the internal pressure. This was achieved by incorporating separate sealing and locking regions in the plug design. The forward end of each plug contains a neck that accommodates a wedge/O-ring set to seal the vessel (Figures 26 and 27). Aft of the seal, hydrostatic pressure effects are mitigated by a hole drilled into the wall of the Mann barrel. Therefore, the forces on the locking threads are longitudinal, and reduce the stress state to a biaxial condition.

Since the threads will be exposed primarily to unidirectional forces, a buttress thread was selected for the closure plug locking section. Essentially, both ends of the Mann barrel are the same. The closure plug at one end allows for the installation of an impactor. The thread stresses were calculated with simple shear load/thread base area formulas (Schigley and Mitchell, 1983).

The wedge/O-ring seals used in the closure plugs are relatively simple in concept. Two complementary rings with a right triangular cross-section are used to sandwich an O-ring, as is shown in Figure 28. The O-ring will be permanently deformed by the wedge rings, which compress the rubber O-ring to achieve a seal. The surface finishes

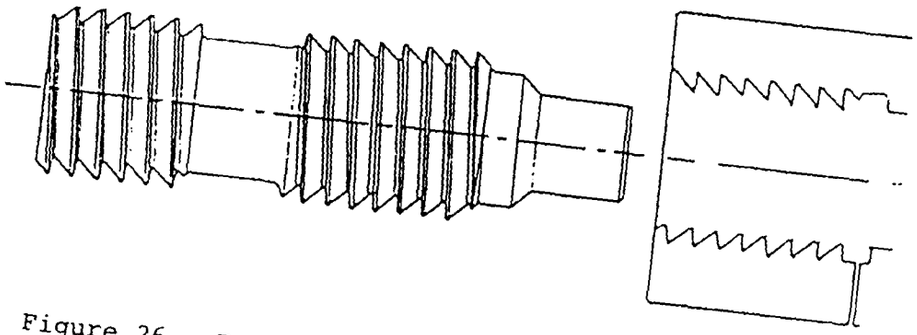

Figure 26. Forward plug with seal area shown.

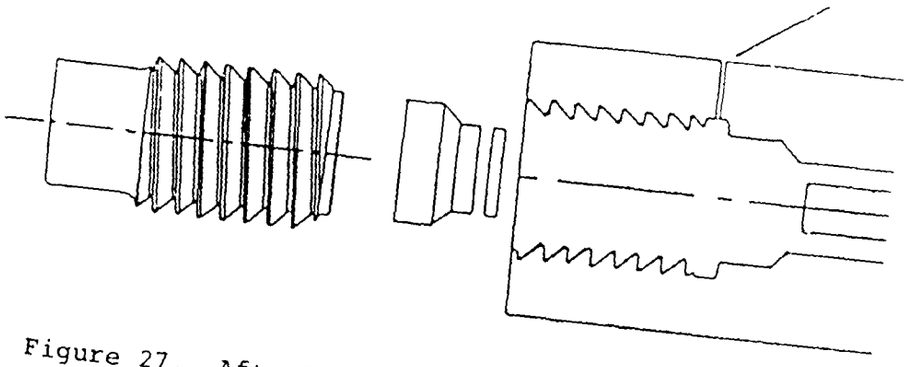

Figure 27. Aft plug (wedge ring seat is located on the electrical feedthrough base).

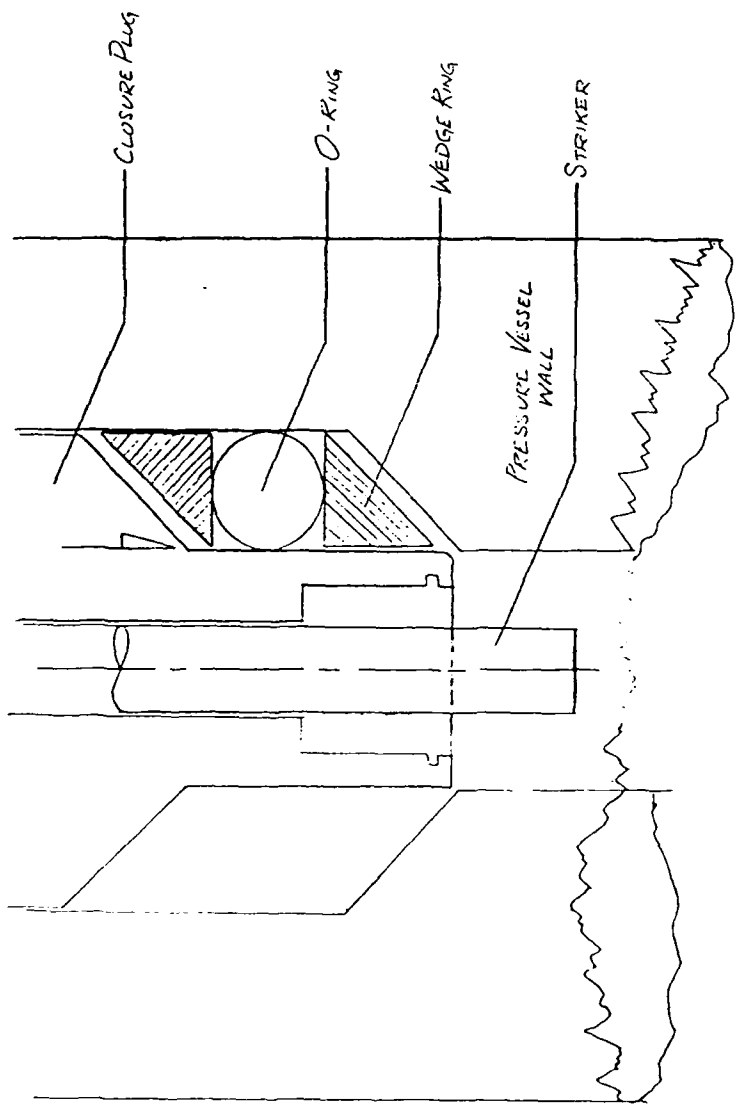

Figure 28. Wedge ring seat detail.

for the seal areas specified in the design were check 16 or better. The seal design for the impactor uses a commercially available piston seal type requiring exceptionally fine machining tolerances. The design specifies the use of Parback seals from Parker Seals Corporation, although any similar seal design should suffice.

The striker is retained by a retainer cap, utilizing the same buttress thread design (the thread direction is the same as the plug threads to ensure that tightening the retainer cap also tightens the closure plug. The material specified for both the cap and plug is 4340 steel (Figures 29 and 30).

The striker material was specified as 7075-T6 aluminum alloy. A shoulder is incorporated in the design to prevent ejection by the confinement pressure (Figure 29). The design specifies radii to reduce stress concentration at the shoulder. The dimensions of the shoulder were developed using shear area calculations:

Shear area = π (0.5) L (where L is the shoulder depth)

Pressure P = 207 MPa (30,000 psi)

Force on Impactor = $P*A_{face}=30x10^3 \times 2\pi(0.25)^2=1.18x10^4$lbf

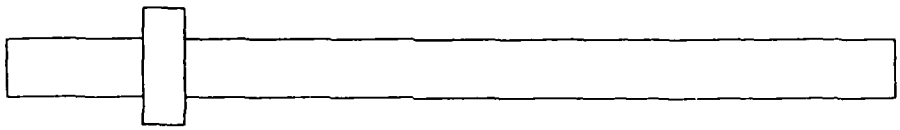

Figure 29. Striker design.

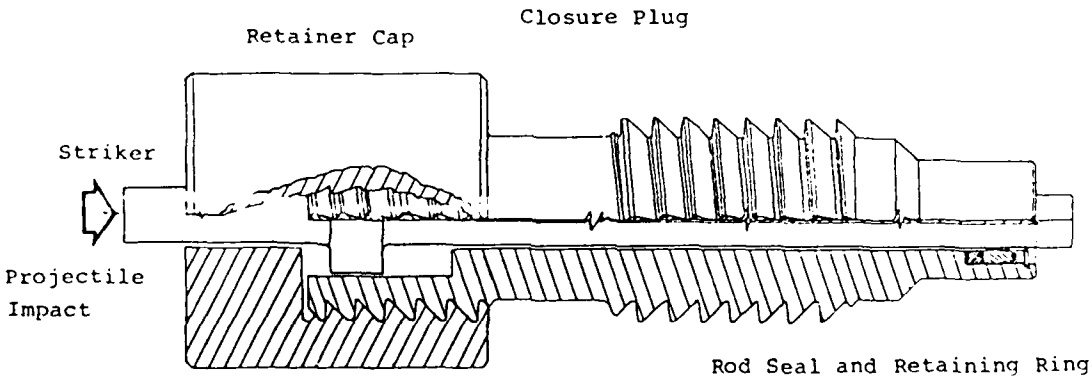

Figure 30. Forward closure plug assembly.

The other closure plug basically acts to seal the vessel, but also must allow passage of electrical conductors associated with bar instrumentation. The conceptual configuration for the feedthrough design was adapted from a ball and seat design developed by Downs and Payne (1969). The design employs a 3-mm-diameter ball bearing which acts as a conductor and provides a sealing surface (Figure 31). The ball bearings are held in place by a plate with semi-spherical impressions machined into the contact surface. The design allows relatively inexpensive construction while maintaining a controlled sealing capability. The feedthrough base seals the pressure vessel with the same wedge/O-ring design as is used on the impactor end and is retained by a threaded, hollow plug.

The device is assembled as follows:

1) The output bar is mounted in the pressure vessel on the spacer rings, then strain gage leads are connected to the feedthrough leads;

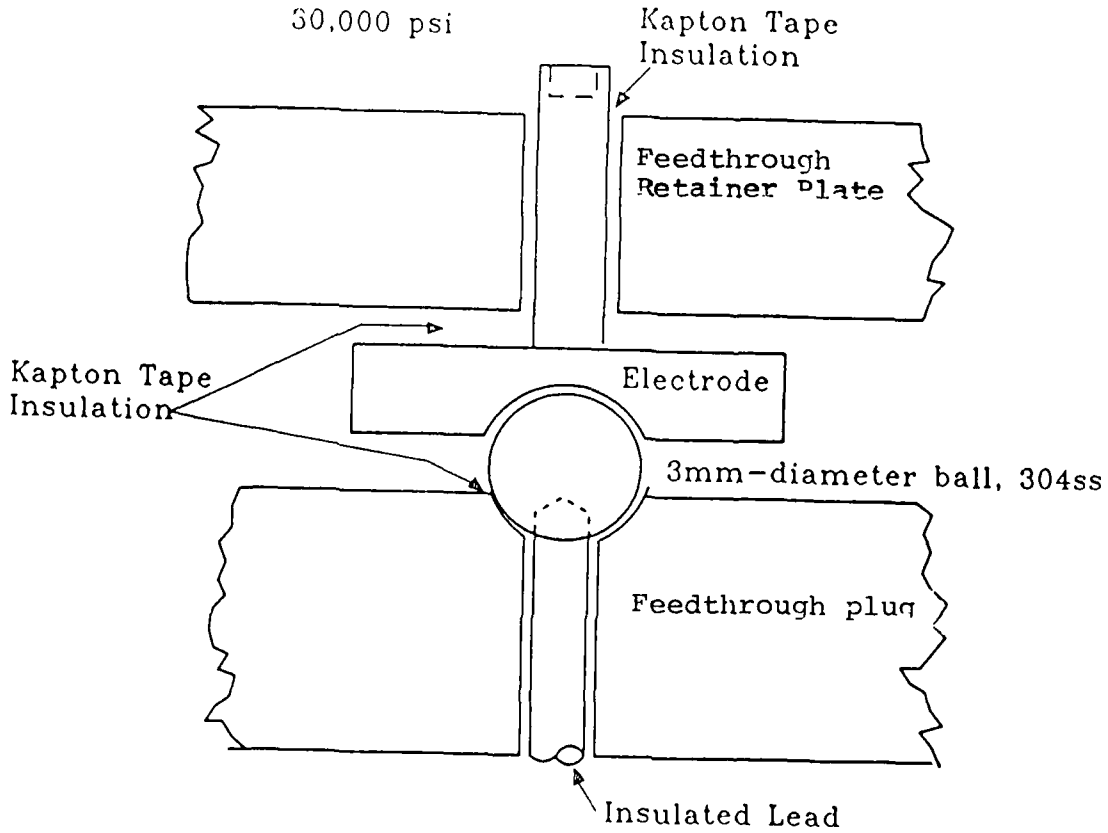

Figure 31. Aft closure plug and electrical feedthrough design.

$$\text{Shear} = \frac{1.18\times10^{4}}{0.5\pi L} = \frac{7500}{L} \; ; \; \tau_{allowable} = \frac{\tau_y}{5} = 48 \text{ MPa (7,000 psi)}$$

therefore, L = 24 mm (0.93 in.).

The other closure plug basically acts to seal the vessel, but also must allow passage of electrical conductors associated with bar instrumentation. The conceptual configuration for the feedthrough design was adapted from a ball and seat design developed by Downs and Payne (1969). The design employs a 3-mm-diameter ball bearing which acts as a conductor and provides a sealing surface (Figure 31). The ball bearings are held in place by a plate with semi-spherical impressions machined into the contact surface. The design allows relatively inexpensive construction while maintaining a controlled sealing capability. The feedthrough base seals the pressure vessel with the same wedge/O-ring design as is used on the impactor end and is retained by a threaded, hollow plug.

The device is assembled as follows:

1) The output bar is mounted in the pressure vessel on the spacer rings, then strain gage leads are connected to the feedthrough leads;

2) The aft end closure/feedthrough is assembled, including the electrodes, electrode retainer, wedge rings,

bar energy absorber, and O-ring;

3) The aft end closure is installed;

4) The specimen is placed on the specimen carrier attached to the active end of the input bar, the input bar is placed in the pressure vessel, and the input bar strain gage leads are attached to the input bar feedthrough leads;

5) The forward end closure/striker is assembled, consisting of wedge rings, O-ring, striker, striker energy absorber, striker seal and seal-back-up ring, snap ring and washer, and retainer cap;

6) The closure plug/striker assembly is installed, sealing the forward end of the vessel. The vessel is then purged with nitrogen and pressurized.

References

1. A. W. Horst, "The Role of Propellant Mechanical Properties in Propelling Charge Phenomenology," U.S. Army Ballistics Research Laboratory, Aberdeen Proving Ground, MD, in CPIA Publication 351, 1981 JANNAF Structures and Mechanical Behavior Subcommittee Meeting, Vol. I, pp. 141-154, December 1981.

2. C. W. Fong, "Crack Initiation in Perforated Propellants Under High Strain Rate Impact Conditions," Weapons Research Laboratory, Defence Research Centre, Salisbury, Adelaide, South Australia, in Propellants, Explosives, and Pyrotechnics, Vol. 10, pp. 91-96 (1985).

3. J. Pinto, S. Nicolaides, D. Georgevich, and D. A. Wiegand, "Mechanical Properties of Candidate LOVA and Nitrocellulose Base Gun Propellants after up to 18 Months of Accelerated (High Temperature) Aging," U.S. Army Research and Development Center, Dover, NJ; in 1983 JANNAF Structures and Mechanical Behavior Subcommittee Meeting, CPIA Publication 388, November 1983, pp. 267-274.

4. M. Costantino and D. Ornellas, "The High Pressure Failure Curve for JA-2," Lawrence Livermore National Laboratory, Livermore, CA; in 1987 JANNAF Structures and Mechanical Behavior Subcommittee Meeting, CPIA Publication 463, March 1987, pp. 73-79.

5. M. Costantino and D. Ornellas, "Initial Results for the Failure Strength of a LOVA Gun Propellant at High Pressures and Various Strain Rates," Lawrence Livermore National Laboratory, Livermore, CA; in 1985 JANNAF Propulsion Meeting, CPIA Publication 425, Vol. I, April 1985, pp. 213-227.

6. R. J. Lieb and J. J. Rocchio, "High Strain Rate Mechanical Properties Testing on Lots of Solid Gun Propellant with Deviant Interior Ballistic Performance," U.S. Army Ballistic Research Laboratory; in 1982 JANNAF Structures and Mechanical Behavior Subcommittee, CPIA Publication 368, October 1982, pp. 23-38.

7. R. J. Lieb, D. Devynck, and J. J. Rocchio, " The Evaluation of High Rate Fracture Damage of Gun Propellant Grains," U.S. Army Ballistic Research Laboratory, Aberdeen Proving Ground, MD; in 1983 JANNAF Structures and Mechanical Behavior Subcommittee, CPIA Publication 388, November 1983, pp. 177-196.

8. R. J. Lieb, J. J. Rocchio, and A. A. Koszoru, "Impact Mechanical Properties Tester for Gun Propellant," U.S. Army Ballistic Research Laboratory, Aberdeen Proving Ground, MD; in 1981 JANNAF Structures and Mechanical Behavior Subcommittee, CPIA Publication 351, December 1981, pp. 155-172.

9. H. Kolsky, "An Investigation of the Mechanical Properties of Materials at Very High Rates of Loading," in Proceedings of the Royal Society, Vol. 62, 1949, pp. 676.

10. R. M. Davies, " A Critical Study of the Hopkinson Pressure Bar," Philosophical Transactions Acta., Vol. 240, 1948, p. 375.

11. F. E. Hauser, "Techniques for Measuring Stress-Strain Relations at High Strain Rates," Experimental Mechanics, Vol. 6, 1961, p. 395.

12. H. Kolsky, Stress Waves in Solids, Dover Publications, New York, NY, 1963.

13. K. G. Hoge, "The Behavior of Plastic-Bonded Explosives Under Dynamic Compressive Loads," Lawrence Livermore Laboratory, Livermore, CA, UCRL-70074, 3 February 1967. 46 pp.

14. K. G. Hoge, "Dynamic Tensile Strength of Explosive Materials," Lawrence Radiation Laboratory, Livermore, CA, 25 February 1970.

15. H. Schubert and D. Schmitt, "Embrittlement of Gun Powder," in Proceedings of the International Symposium on Gun Propellants, Dover, NJ, October 1973.

16. P. J. Greidenus, "Simple Determination of the Mechanical Behavior of Double-base Rocket Propellants Under High Loading Rates," in AGARD 47th Meeting, Propulsion and Energetics Panel, Paper 23, FRG, May 1976.

17. P. Benhaim, J. L. Paulin, and B. Zeller, "Investigation on Gun Propellant Breakup, and Its Effect in Interior Ballistics," in Proceedings of the 4th

International Symposium on Ballistics, Monterey, CA, October 1978.

18. W. J. Murri, Y. Horie, and D. R. Curran, "Dynamic Fracture Experiments on VRA Propellants," Lawrence Livermore Laboratory, Livermore, CA, June 1977, UCRL-15550.

19. R. A. Wires, J. Pfau, and J. J. Rocchio, "The Effects of High Rates of Applied Force and Temperature on the Mechanical Properties of Gun Propellants," in 1979 JANNAF Propulsion Meeting, Vol. I, CPIA Publication 300, pp. 25-50, March 1979.

20. J. E. Schigley, and L. D. Mitchell, Mechanical Engineering Design, 4th Ed., McGraw-Hill, New York, NY, 1983.

21. S. Timoshenko and J. N. Goodier, Theory of Elasticity, 3rd Ed., McGraw-Hill, New York, NY, 1970.

22. T. Baumeister, E. A. Avallone, and T. Baumeister, Mark's Standard Handbook for Mechanical Engineers, 8th Edition, McGraw-Hill, New York, NY, 1978.

23. J. L. Downs and R. T. Payne, "A Review of Electrical Feedthrough Techniques for High Pressure Gas Systems," in The Review of Scientific Instruments, Vol. 40, Number 10, October 1969.

24. R. J. Christensen, S. R. Swanson, and W. S. Brown, "Split-Hopkinson Bar Tests on Rock Under Confining Pressure," in Experimental Mechanics, November 1972, pp. 508-513.

25. J. D. Chalupnik and E. A. Ripperger, "Dynamic Deformation of Metals Under High Hydrostatic Pressure," in Experimental Mechanics, Vol. 6, Number 11, pp. 547-554, 1966.

26. E. James and D. Breithaupt, High Strain Rate Mechanical Testing of Solid Propellants by the Hopkinson Split Bar Technique, Lawrence Livermore National Laboratory, UCID-20021, 16 February 1984.

27. Marsh, B. P., "The Effects of Specimen Size on the Mechanical Properties of a Composite Propellant," U.S. Army Missile Command, Redstone Arsenal, AL, in 1987 Structures and Mechanical Behavior Subcommittee Meeting, March 1987, pp. 41-50, CPIA Publication 463.

INITIAL DISTRIBUTION

- Army -

ARDEC/PICATINNY ARSENAL
1 DR. ANTHONY J. BEARDELL
1 DR. JOSEPH A. LANNON
1 A. R. LUSARDI
1 SPERO NICOLAIDES
1 DR. JEAN-PAUL PICARD
2 SMCAR-MSI-I

ARDEC/WATERVLIET
1 SMCAR-LCB-TL

ARMAMENT MUNITIONS CHEM COMD/ROCK ISLAND
1 ROBERT GUNNARI
1 MR. PETER W. HOGBERG
1 P. E. KROUSE

ARMY AIR DEF ARTY SCH/FORT BLISS
1 ATSA-SEL-DOC SEC

ARMY ANV RSCH & TECH ACTV/FORT EUSTIS
1 SAVRT-TY-TSC-TECH LIB

ARMY BALLISTIC RESEARCH LABS/ABERDEEN
1 DR. AUSTIN W. BARROWS
1 JOHN M. HURBAN
1 LOUISE LETENDRE
1 INGO W. MAY

ARMY BELVOIR R&D COMD/FORT BELVOIR
1 F. SCHAEKEL

ARMY COMD STAFF COLLEGE/FT LEAVENWORTH
1 ATZL-SWS-L

ARMY DEF AMMO CTR SCH/SAVANNA
1 A. H. BAUSMAN

ARMY FGN SCI TECH CTR/CHARLOTTESVILLE
1 JAMES HEADDEN

ARMY LABORATORY COMD/WATERTOWN
1 M. M. MURPHY

ARMY MAT SYS ANALYSIS/ABERDEEN
1 AMXSY-PS-SCTY MGR

ARMY MED BIOENG R&D LAB/FREDERICK
1 SGRD-UBZ-A E. M. SNYDER

ARMY MSL COMD/REDSTONE ARSENAL
1 BERNARD J. ALLEY
1 DOCUMENTS, AMSMI-RD-CS-R
1 ROBERT E. BETTS
1 DAVID R. DREITZLER
1 FRANCIS E. HART
1 DONALD J. IFSHIN
1 DR. JAMES A. MURFREE, JR.
1 MR. J. MICHAEL LYON
1 ALBERT R. MAYKUT
1 MR. J. KERMIT MITCHELL
1 RICHARD A. REYNOLDS
1 DR. RICHARD G. RHOADES
1 DONALD P. SHEPHERD
1 DR. WILLIAM D. STEPHENS
1 H. C. STILL
1 ARNOLD T. STOKES
1 JOHN M. TATE
1 TERRY L. VANDIVER
1 BEN F. WILSON

ARMY RSCH OFC/RESEARCH TRIANGLE PARK
1 DRXRO-PP-LIB
1 D. M. MANN

ARMY STRATEGIC DEF COMD/HUNTSVILLE
1 A. B. DUMAS
1 D. C. SAYLES

HARRY DIAMOND LABORATORIES/ADELPHI
1 L. RYAN

PLASTICS TECH EVAL CTR/DOVER
1 H. E. PEBLY

RADFORD ARMY AMMO PLANT/RADFORD
1 SMCRA-QA

WHITE SANDS MISSILE RANGE/WHITE SANDS
1 TECH LIB

- Navy -

DAVID TAYLOR NAVAL SHIP R&D/ANNAPOLIS
1 N. HATFIELD

DAVID TAYLOR NAVAL SHIP R&D/BETHESDA
1 CODE 5221--TECH INF LIBS

NAVAL AIR PROPULSION CTR/TRENTON
1 LIBRARY

NAVAL AIR SYS COMD/WASHINGTON, DC
1 G. E. KOVALENKO
2 AIR-5004-TECH LIB
1 NAIR-5304
1 NAIR-53713
1 BERTRAM P. SOBERS

NAVAL COASTAL SYS CTR/PANAMA CITY
1 TECH INFO SVCS, CODE 6120

NAVAL EXPLO ORD DSPL FAC/INDIAN HEAD
1 LIB DIV

NAVAL INTEL SPT CTR/WASHINGTON, DC
1 LESLIE KUSHNER
1 DOC LIB

NAVAL ORD STATION/INDIAN HEAD
1 RAY H. BAZIL
1 W. E. BROWN
1 MS. LINDA MILLAR
1 C. PARAS
1 F. VALENTA

NAVAL ORDNANCE STATION/INDIAN HEAD
4 CHARLES GALLAGHER
1 MR. CARL GOTZMER
1 DR. AETIUS R. LAWRENCE

NAVAL ORDNANCE STATION/LOUISVILLE
1 CODE 50-D

NAVAL POSTGRADUATE SCHOOL/MONTEREY
1 CODE 1424--LIBS DIR

NAVAL RSCH LAB/WASHINGTON, DC
2 CODE 2627
1 CODE 6100
1 V. J. KUTSCH

NAVAL RSCH/ARLINGTON
1 DR. RICHARD S. MILLER

NAVAL SEA SYS COMD/WASHINGTON, DC
1 ROBERT F. CASSEL
1 MR. CHARLES M. CHRISTENSEN
1 E. KRATOVIL
1 REX M. LARSEN
1 SEA-09B312--TECH LIB
1 ELGIN WERBACK

NAVAL SHIP WPN SYS ENG STA/PORT HUENEME
1 CODE 4G00, VIA J.D. FLANAGAN
1 CODE 02, VIA J.D. FLANAGAN

NAVAL SURFACE WARFARE CTR/DAHLGREN
2 TECH SERVICES, CODE E231
1 JESSE L. EAST

NAVAL SURFACE WARFARE CTR/SILVER SPRING
1 RICHARD R. BERNECKER
1 DR. ROBERT J. EDWARDS
3 S. HAPPEL
1 MR. CHARLES R. ROWE

NAVAL UNDERWATER SYS CMD/NEWPORT
1 TECH LIB 021312

NAVAL WPN CTR/CHINA LAKE
1 CODE 3274
1 CODE 327
3 CODE 3431
1 CODE 389
1 JAMES C. BALDWIN
1 THOMAS L. BOGGS
1 GEORGE W. BURDETTE
1 DR. MAY L. CHAN
1 LEE N. GILBERT
1 DR. GEOFFREY A. LINDSAY
1 JAMES A. LOUNDAGIN
1 C. FRANK MARKARIAN
1 JACK M. PAKULAK
1 MARY S. PAKULAK
1 DR. RUSSELL REED
1 ROBERT T. REID
1 DR. KLAUS C. SCHADOW
1 ALFRED O. SMITH
1 ANDREW C. VICTOR
1 FREDERICK C. ZARLINGO

NAVAL WPN SPT CTR/CRANE
1 B. E. DOUDA

NAVAL WPN STA/CONCORD
1 T. W. LOHRMANN

NAVAL WPN STA/SEAL BEACH
1 MICHAEL SADOSKI

NAVY STRAT SYS PROJ OFC/WASHINGTON, DC
1 MR. MICHAEL BARON
1 TECH LIB BR HD
1 MR. E. LEROY THROCKMORTON

PACIFIC MISSILE TEST CTR/POINT MUGU
1 TECH LIB

U. S. NAVAL ACADEMY/ANNAPOLIS
1 R. A. EVANS

- Air Force -

6520 TESTG/EDWARDS AFB
1 TECH LIB--STOP 238

AAMRL/WPAFB
1 TH

AEDC/ARNOLD AFS
1 TECH LIB

AFAL/EDWARDS AFB
1 DR. CLARK W. HAWK STOP 24
1 JOHN H. CLARK
1 ROBERT C. CORLEY
1 DR. DAWEEL GEORGE
1 JAMES L. KOURY
1 TECH LIB
1 LK
1 JOHN W. MARSHALL
1 LEE G. MEYER
1 MKA
1 MKP
1 DR. FRANCIS Q. ROBERTO
1 WAYNE E. ROE
1 MELVIN V. ROGERS
1 DURWOOD I. THRASHER
1 DAVID P. WEAVER
1 DR. RICHARD R. WEISS

AFSC/WASHINGTON, DC
1 RICHARD E. SMITH

AFWAL/WPAFB
1 CHARLES S. ANDERSON
1 WILLIAM G. BEECROFT
1 DR. EDWARD T. CURRAN
1 JACK R. FULTZ
1 POPS
1 JAMES W. SUMMITT
1 LEO SCOTT THEIBERT

AFWL/KIRTLAND AFB
1 SUL-TECH LIB

AMD/BROOKS AFB
1 COL. D. C. BEATTY
1 COL. C. B. HARRAH

ASD/WPAFB
2 XRHI--PROPULSION GROUP
1 DALE HANKINS
1 WILLIAM PRICE

BMO/NORTON AFB
1 WALLY CARTER

ETR/PATRICK AFB
1 R. SZYNAKA

FTD/WPAFB
1 CAPT. DAWN ADAMS
1 ARNOLD CROWDER
1 D. HOHLER
1 RON MOREDOCK

SAC/OFFUTT AFB
1 NRI-STINFO

WSMC/VANDENBERG AFB
1 SAMTEC-SE

- NASA -

NASA FLIGHT RSCH CTR/EDWARDS
1 LIB

NASA GODDARD/GREENBELT
1 LIB

NASA JOHNSON SPACE CTR/HOUSTON
1 THOMAS GRAVES

NASA JSC WSTF/LAS CRUCES
1 IRVIN D. SMITH

NASA LANGLEY/HAMPTON
1 ROBERT A. JONES
1 F. S. KIRKHAM
2 MS-185 TECH LIB
1 MR. MELVIN LUCY
1 DR. G. BURTON NORTHAM

NASA LEWIS RSCH CTR/CLEVELAND
3 D. MORRIS
1 G. M. RECK

NASA LEWIS/CLEVELAND
1 L. A. DIEHL
1 M/S 500-218, W. A. THOMAS

NASA SCI TECH INF FAC/BWI
1 ACCESSIONING DEPT

NASA WALLOPS FLT CTR/WALLOPS ISLAND
1 JANE N. FOSTER

NASA/KENNEDY SPACE CENTER
1 MD-ESB, A. M. KOLLER

NASA/MARSHALL SPACE FLIGHT CENTER
1 AS24D
1 J. O. FUNKHOUSER

NASA/MARSHALL SPACE FLIGHT CTR
1 CN22/LIBRARY
1 MR. ROBERT J. RICHMOND

NASA/WASHINGTON, DC
1 JOHN SCHELLER, CODE MVS
1 W. R. FRAZIER, CODE QSO
1 ADMIN DIV NHB-12 LIB SEC

- Other Gov't. -

CENTRAL INTEL AGCY/WASHINGTON, DC
1 OCR/DSD/DLB

DEF INTEL AGENCY/WASHINGTON, DC
1 P. MURAD, DT4A

DEF TECH INFO CTR/ALEXANDRIA
1 WILLIAM BARNES
2 DTIC-DDA
1 DTIC-HAR

SECRETARY OF DEFENSE/WASHINGTON, DC
1 DR. L. H. CAVENY, SDIO/IST

UNDER SEC OF DEF ACQ/WASHINGTON, DC
1 DR. DONALD DIX

- Non-Gov't. -

AEROJET GENERAL/SACRAMENTO
1 TECH INF CTR

AEROJET/SACRAMENTO
1 R. MIRONENKO

AEROSPACE/LOS ANGELES
1 S. B. CROWE

AIR PRODUCTS & CHEMICALS/ALLENTOWN
1 C. E. ANDERSON

ATLANTIC RESEARCH/GAINESVILLE
2 TECHNICAL INF CTR

AVCO/WILMINGTON
1 E. D. HOWARD

BOEING/SEATTLE
2 8K-38 LIB PROC SUPV

CALIFORNIA INST TECHNOLOGY/PASADENA
1 LIB ACQS/STANDING ORDERS

FMC CORP/MINNEAPOLIS
2 C. AUGENSTEIN

FORD AEROSPACE/NEWPORT BEACH
1 TECH INF SVC--DDC ACQS

GENERAL DEFENSE/RED LION
1 MR. HUGH MCELROY

GENERAL DYNAMICS/POMONA
1 MZ-4-20-CH LIB

GRUMMAN AEROSPACE/BETHPAGE
1 HAROLD B. SMITH

HERCULES/MAGNA
1 C. F. PARTRIDGE

HERCULES/MCGREGOR
1 BLDG A-100

HERCULES/ROCKET CENTER
1 LIB

HUGHES AIRCRAFT/EL SEGUNDO
2 DOROTHY WEBB

JHU/APL
1 FREDERICK S. BILLIG
1 MARK GRUBELICH, 10A-120
1 JAMES GEORGE, 6-381
1 JOHN EICHSTEDT, 8-242

LOCKHEED MSL & SPACE/PALO ALTO
1 MR. CHARLES LEONG

LORAL/AKRON
1 LIB

LTV MISSILES & ELCT GP/DALLAS
2 LIB 3-58210, MAIL STOP EM-08

MARQUARDT/VAN NUYS
1 LYDIA LEE
1 LIB

MCDONNELL DOUGLAS/ST. LOUIS
1 C. L. LAUER

MORTON THIOKOL/BRIGHAM CITY
1 J. E. HANSEN

MORTON THIOKOL/ELKTON
1 D. J. MCDANIEL

MORTON THIOKOL/HUNTSVILLE
1 C. S. WECKWARTH

MORTON THIOKOL/OGDEN
1 T. F. DAVIDSON

OLIN/CHESHIRE
1 DAVID F. GAVIN

OLIN/MARION
1 M. R. RHINE

OLIN/ST. MARKS
1 E. J. KIRSCHKE

PENNSYLVANIA STATE UNIV/STATE COLLEGE
1 DANIEL KIELY
1 K. K. KUO

PRINCETON COMBUSTION/MONMOUTH JUNCTION
1 N. A. MESSINA

RAYTHEON/BEDFORD
1 J. DURBEN

ROCKWELL/CANOGA PARK
1 TECH INF CTR

ROCKWELL/DOWNEY
1 TIC-D201-300-AJ01

SANDIA NATIONAL LABS/ALBUQUERQUE
1 LIB 3141, CARMEN WARD

SOUTHWEST RESEARCH INSTITUTE/SAN ANTONIO
1 DR. HAROLD J. GRYTING

SRI INTERNATIONAL/MENLO PARK
1 CLASSIFIED DOC SVC

STONE ENGINEERING/HUNTSVILLE
1 D. OWENS

TALLEY/MESA
1 SECURITY OFFICE

TELEDYNE MCCORMICK SELPH/HOLLISTER
1 GEOFF ARNOLD

TEXTRON/BUFFALO
1 L. M. BRESLAUER

TEXTRON/EVERETT
1 L. T. NAZZARO

TRW/REDONDO BEACH
1 WEYMAN KAM, SAN BERNARDINO
1 S/1930
1 A. E. SAMSONOV

UNIDYNAMICS/PHOENIX
1 C. RITTENHOUSE

UNITED TECHNOLOGIES/EAST HARTFORD
1 M. E. DONNELLY

UNITED TECHNOLOGIES/SAN JOSE
1 TECHNICAL LIBRARY

UNIVERSAL PROPULSION/PHOENIX
1 H. J. MCSPADDEN

UNIVERSITY CALIFORNIA/LIVERMORE
1 M. J. HIGBY